



Original Paper

3D Integrated Structural, Facies and Petrophysical Static Modeling Approach for Complex Sandstone Reservoirs: A Case Study from the Coniacian–Santonian Matulla Formation, July Oilfield, Gulf of Suez, Egypt

Ahmed M. Ali,¹ Ahmed E. Radwan ,^{2,3,5} Esam A. Abd El-Gawad,⁴ and Abdel-Sattar A. Abdel-Latief¹

Received 11 August 2021; accepted 4 November 2021
Published online: 2 December 2021

The Coniacian–Santonian Matulla Formation is one of the important reservoirs in the July oilfield, Gulf of Suez Basin. However, this formation is characterized by uncertainty due to the complexity of reservoir architecture, various lithologies, lateral facies variations and heterogeneous reservoir quality. These reservoir challenges, in turn, affect the effectiveness of further exploitation of this reservoir along the Gulf of Suez Basin. In this work, we conduct an integrated study using multidisciplinary datasets and techniques to determine the precise structural, petrophysical, and facies characteristics of the Matulla Formation and predict their complex geometry in 3D space. To complete this study, 30 2D seismic sections, five digital well logs, and core samples of 75 ft (ft = 0.3048 m) length were used to build 3D models for the Matulla reservoir. The 3D structural model shows strong lateral variation in thickness of the Matulla Formation with NW–SE, NE–SW and N–S fault directions. According to the 3D facies model, shale beds dominate the Matulla Formation, followed by sandstone, carbonate, and siltstone beds. The petrophysical model demonstrates the Matulla reservoir's ability to store and produce oil; its upper and lower zones have good quality reservoir, whereas its middle zone is a poor quality reservoir. The most promising areas for hydrocarbon accumulation and production via the Matulla reservoir are located in the central, southeast, and southwest sectors of the oilfield. In this approach, we combined multiple datasets and used the most likely parameters calibrated by core measurements to improve the reservoir modeling of the complex Matulla reservoir. In addition, we reduced many of the common uncertainties associated with the static modeling process, which can be applied elsewhere to gain better understanding of a complex reservoir.

¹Department of Geology, Faculty of Science, Al-Azhar University, Assiut Branch, Assiut 71524, Egypt.

²Faculty of Geography and Geology, Institute of Geological Sciences, Jagiellonian University, Gronostajowa 3a, 30-387 Kraków, Poland.

³Exploration Department, Gulf of Suez Petroleum Company (GUPCO), Cairo, Egypt.

⁴Department of Geology, Faculty of Science, Al-Azhar University, Nasr City, Cairo 11884, Egypt.

⁵To whom correspondence should be addressed; e-mail: radwanae@yahoo.com

KEY WORDS: 3D modeling, 3D Structural modeling, 3D Petrophysical modeling, Volumetric modeling, Facies modeling, Reservoir characterization, Reservoir architecture, Reservoir quality, Gulf of Suez.

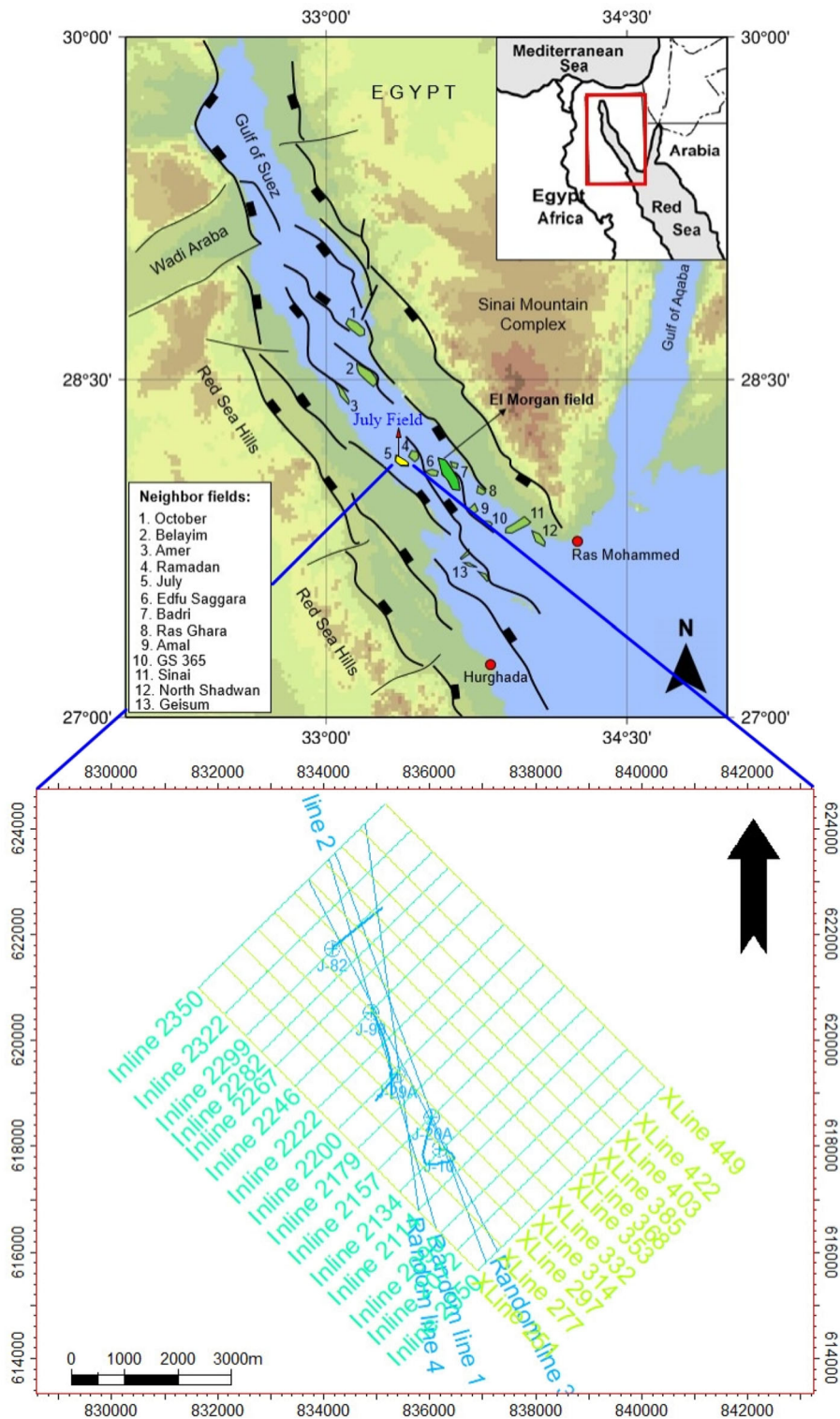
INTRODUCTION

The current research developments within the energy sector are seeking better exploitation of subsurface resources through enhancement of resource prediction and efficient production. This can be achieved by accurate modeling of the rock physical and fluid characteristics in 3D space in order to improve production efficiency and resource recovery (Radwan, 2022; Wu & Xu, 2004, 2005; Yan-Lin et al., 2011). Three-dimensional (3D) modeling of hydrocarbon reservoirs is the key factor that controls hydrocarbon reservoir evaluation and simulation for better exploitation and successful development. Although, 3D geological modeling can be done in oil and gas reservoirs easily using various available software, the modeling accuracy still presents a big challenge that has a great impact on the effective development of hydrocarbon reservoirs (Abdel-Fattah et al., 2010, 2018 Bilodeau et al., 2002; Bryant & Flint, 1993, 2009; Radwan, 2022). Multi-source data can be integrated into the reservoir's 3D geological property models. The geological model allows attributes to be assigned to each cell, and the quantitative reservoir models are often cell-dependent. Such models place far greater challenges on the geologist than conventional models do because geology requires a complete explanation at any point within a reservoir's 3D volume. Multi-integrated properties can be used to define a 3D geological model, which is critical for connecting data from a wellbore to a 3D geological model in order to create efficient reservoir simulations (Abdelmaksoud et al., 2019a; Abu Amarah et al., 2019; Cosentino, 2005; Deutsch, 2002; Doyen, 2007; Qadri et al., 2019; Radwan, 2022). The main advantage of 3D modeling approaches is the ability to model complex reservoirs with variable lithologies and reservoir heterogeneities, and so accurate parameters and the best data integration are required for better reservoir modeling.

The Coniacian–Santonian deposits of the Matulla Formation are part of the Nezzazat Group, and they are distinguished by various lithologies, lateral

facies and thickness changes, and reservoir heterogeneities across the Gulf of Suez basin (Fig. 1) (Alsharhan, 2003; El-Sabbagh et al., 2011; Kassem et al., 2020; Shehata et al., 2021). In Gabal Nezzazat, Sinai, the Matulla Formation is a well-exposed siliciclastic/carbonate facies (El-Azabi & El-Araby, 2007; Said, 1990). The Matulla reservoir is the third most important reservoir in the July oilfield (Fig. 1), following the Rudies and Nubia Sandstone reservoirs (EGPC, 1996). The structural and stratigraphic framework of the exposed Matulla Formation was established by El-Azabi and El-Araby (2007), Hasouba et al. (1992) and Marttila and El Bahr (1994). Due to reservoir heterogeneities and lateral facies changes in the Matulla sandstone reservoir, major exploration problems were encountered during its exploitation in the basin, posing a challenge and increasing exploration risks. In this regard, precise subsurface area modeling is required to solve the reservoir architecture in the July oilfield.

The ultimate goal of this study was to provide a new set of potentially optimistic reservoir targets for modeling hydrocarbon accumulation and reservoir characteristics in the complex and heterogeneous Matulla reservoir, using precise 3D modeling with low uncertainties. To overcome the associated facies changes and reservoir complexity of Matulla in the subsurface of the July oilfield, the reservoir architecture, petrophysical parameters, structural characteristics, and facies distribution must be understood and recognized. Simulation of complex reservoir property was used in this work to populate the grid cells of a 3D model with integrated constructed (structural modeling), discrete (facies modeling), and continuous properties (petrophysical modeling). Therefore, we utilized available data from 2D seismic reflection sections, wireline logs, and core sample analysis to define the main structural characteristics of the study area, recognize the distribution of the thickness/facies of the Matulla Formation reservoir, and evaluate its petrophysical perspective. Moreover, we applied best-fit parameters in the reservoir simulation to decrease final geological model uncertainties.



◀ **Figure 1.** Location map of the studied area showing the positions of the studied 30 seismic lines and five wells.

GEOLOGIC SETTING OF THE STUDY AREA

The Gulf of Suez rift is an extended graben shaped by Oligocene rifting as a northern continuation of the Red Sea (Garfunkel & Bartov, 1977; McClay et al., 1998; Radwan et al., 2021a, 2021b, 2021c, 2021d, 2021e). The studied July oilfield is located in the Belayim province (NE-tilted fault blocks and SW-dipping normal faults), and it is bounded to the north by latitudes 28°13'N and 28°18'N and to the east by longitudes 33°11'E and 33°17'E (Fig. 1) (EGPC, 1996; Gaafar et al., 2009). Day and Hoffman (1997) stated that the July oilfield is a highly faulted, complex structure formed by multiple reservoirs within 46 fault-blocks. Within the oilfield, compartmentalization results in different fluids, production, and depletion characteristics for each reservoir compartment.

An asymmetric NE-dipping tilted fault-block is connected to the SW by a SW-dipping fault, and characterized by large displacement normal faults that form the main part of the July oilfield. The major fault block is subdivided into northern and southern blocks, which have slightly different structural histories and trapping mechanisms, by an ENE-trending cross-fault. Initially, in the Oligocene, transverse movement on the cross-fault occurred, causing uplift of the southern block and erosion prior to Miocene deposition. Another transverse movement occurred in the Miocene (Upper Rudeis), causing uplift of the northern block and truncation of the Lower Rudeis reservoir sandstone on the crest (Brown, 1980).

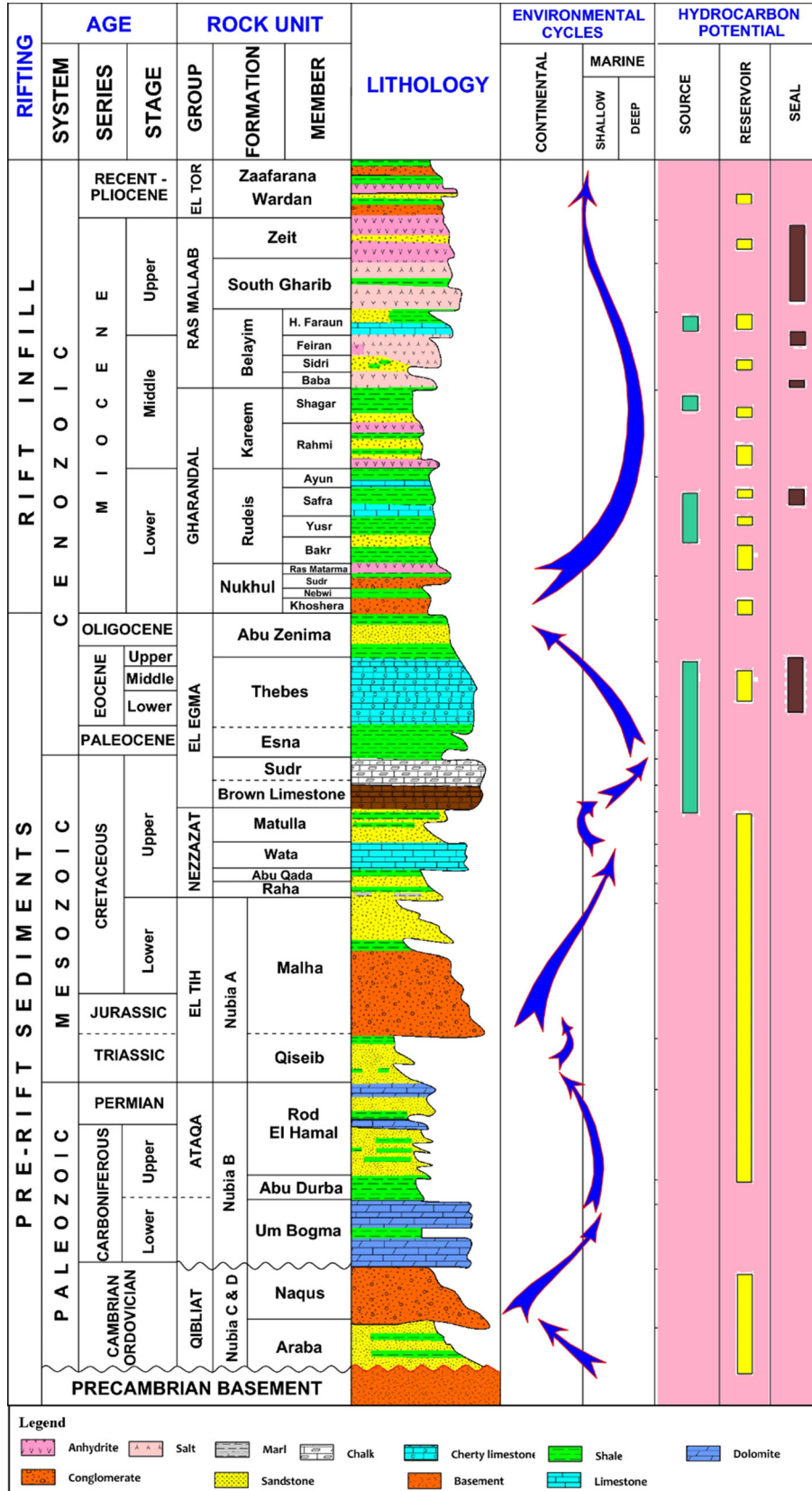
The Gulf of Suez stratigraphy can be divided into three main tectonic stratigraphic successions (Colletta et al., 1988). Some authors describe these successions as lithostratigraphic units (Alsharhan, 2003; Radwan et al., 2021a, 2021b, 2021c, 2021d, 2021e; Said, 1990). They include pre-rift (pre-Miocene) interval (e.g., Radwan et al., 2020b, 2021a), syn-rift (Oligocene–Miocene) interval (e.g., Kassem et al., 2021a, 2021b; Radwan & Sen, 2021a, 2021b, 2021c, 2021d; Shehata et al., 2021), and post-rift (post-Miocene) interval (e.g., Darwish and El Arab, 1993; Radwan, 2020a; 2021a, 2021b, 2021c). The thickness, areal distribution, lithology, hydrocarbon

importance, and depositional environments of these units vary (e.g., Abdelghany et al., 2021; Alsharhan, 2003; Elkhawaga et al., 2021; Radwan et al., 2019a, 2019b, 2019c). In the July oilfield, the sedimentary sequence ranges in age from Paleozoic to Recent (EGPC, 1996). The general stratigraphic section of the July oilfield is shown in Figure 2. According to EGPC (1996), the main reservoirs of the July oilfield are Miocene clastic deposits (Rudeis and Nukhul Formations), pre-Miocene Cretaceous Nezzazat Group, and Nubia Formation. The studied deposits of the Matulla Formation were alternating shallow marine shales, carbonates and sandstones of Upper Cretaceous age (Coniacian–Santonian). The Coniacian–Santonian Matulla Formation is well formed in the southern and central areas of the basin, and it can be divided into three depositional units (M1–M3) (El Sharawy & Nabawy, 2015). An unconformity separates the intermediate unit (M2) and the upper unit (M3) (El Sharawy & Nabawy, 2015).

MATERIALS AND METHODS

The Gulf of Suez Petroleum Company (GUPCO) provided the datasets for the current study as part of an agreement with the Egyptian General Petroleum Corporation (EGPC). Thirty 2D seismic sections were represented by 15 NE–SW direction sections (in-line seismic), 11 NW–SE direction sections (cross-line seismic) and four N–S direction sections (randomly) (Fig. 1). Digital well logs for the July-10, 20A, 29A, 82, and 93 wells were also provided, which include caliper, gamma ray, resistivity, PEF, neutron, density, and sonic datasets. The July-93 well was the only well that was cored within the Matulla Formation section in the central area of the July oilfield. The flowchart of the processing steps used in this work is provided in Figure 3.

During the reservoir 3D modeling process, multi-simulation methods were proposed to understand and model the reservoir. The sequential Gaussian simulation (SGS) method is used widely in reservoir modeling applications (i.e., Petrel™ software) (Hu & Le Ravalec-Dupin, 2005; Isaaks, 1991; Radwan, 2022). The ability to simulate complex structures is the most significant advantage of 3D modeling techniques. The modeling process is divided into several stages beginning with seismic, structural, facies, and petrophysical modeling, then ending with the final interpreted model as the following.



◀ **Figure 2.** Generalized stratigraphic column of the July oilfield (Alsharhan & Salah, 1995; EGPC 1996).

Seismic Interpretation

The interpretation of seismic data is an integral part of the hydrocarbon development strategy of the oilfield. It performs a variety of tasks in 3D seismic interpretation, such as analyzing the parameters that govern reservoir architecture (John et al., 2010; Qadri et al., 2017, 2020). The seismic interpretation, which was based primarily on seismic data provided by the company, included the following.

Performing Seismic to Well Tie

The seismic data are estimated in time domain, and are compared with the well data, which are measured in depth. In this regard, the primary goal of well-to-seismic ties is the correlation of horizon tops that are found in a well with specific seismic reflections. In this study, the data were used to tie well data to seismic are simple because the seismic in depth domain facilitated the connection between wells and seismic lines.

Selecting Studied Horizons on Seismic Sections

Seismic reflection data from every in-line and cross line were interpreted to overcome the data quality issue and retain the precision of horizon and fault interpretation. The interpreted seismic section in different directions is passed near to all wells. All lines intersect in the seismic grid. In this study, we focused on the Matulla Formation, which is the study target.

Interpretation of Faults Affecting These Horizons

Fault movements affect hydrocarbon traps and pathways in addition to deforming sedimentary basins (Gartrell et al., 2004; Radwan et al., 2021c). Thus, fault interpretation is an important part of a structural framework model. Based on the discontinuity in reflection and the abrupt termination of reflection occurrences, the faults present in the study area were established.

Constructing Depth Structure Contour Maps

In the present study, depth structure contour maps were constructed for the Matulla Formation by using Petrel software to illustrate the subsurface structural configuration of the investigated area. The interpreted seismic data were the main container for the 3D geologic modeling (facies and their petrophysical characteristics) according to Radwan (2022). During the 3D structural modeling, the seismic interpretations were the main input data for the Matulla Formation.

Structural Modeling

The second stage of seismic data analysis was the creation of a structural model. The fundamental benefit of a 3D model is that it allows the interpreter to observe and evaluate structural data by displaying a cross section across the model in any direction (Fagin, 1991; Radwan, 2022). A structural model of a reservoir provides borders for the facies and petrophysical models that define the rock qualities, forming the geometrical framework for the 3D grid. The development of a structural model not only allows us to test the model through structural sections, but it also gives us a vision for new well trajectories (Islam, 2021; Qadri et al., 2017; Radwan, 2022), volumetric calculations, and reservoir simulation grids (Holden et al., 2003).

Three major processes were required to complete the structural modeling (i.e., fault modeling, pillar gridding, and horizon generation) (Abdelmaksoud et al., 2019b; Radwan, 2022). The constructed faults were modeled first, whereby this process defined the faults in the geological model and formed the basis for generating the 3D grid, and defined the shape of the faults being modeled by generating the key pillars. Before going to the next step of structural modeling, the key pillars needed some adjustments. A modeled fault must never cross another fault without being connected; however, there were a few cases of crossing faults. The key pillars of the crossing faults were connected in the 3D window, then the pillar gridding process, which involved creating structural grids from the fault model, was carried out. This procedure created the model's skeleton framework. The skeleton grid was made up of three sections: a top, a middle, and a base skeleton grid. Each grid was tied to the essential pillars top, middle, and bottom points. The pillar

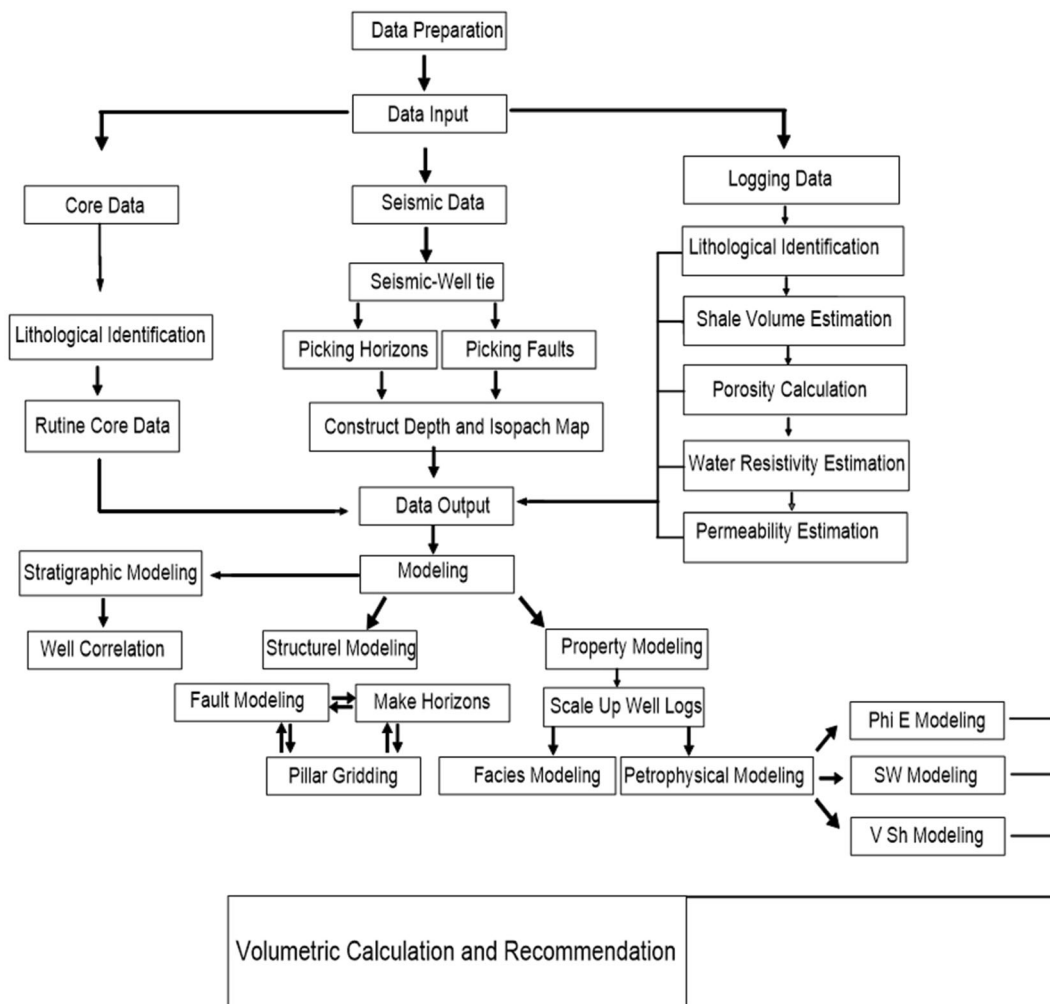


Figure 3. Flowchart of the steps followed in this work.

grid parameters of the study area included a 3D grid increment of 50 m by 50 m and a gridding boundary area limited to depth surfaces. The final step was to create horizons boundaries that denoted the adding of the model's various horizons, which were represented through the Matulla reservoir boundaries (top and bottom) (Abdel-fattah et al., 2010; Abdelmaksoud, 2017; Ali et al., 2019b; Avseth et al., 2005; Cannon, 2018; Cosentino, 2005; Radwan, 2022).

Petrography and Facies Analysis

The petrography is important in well logging because it provides evidence of the mineralogical composition that can affect log reaction (Abudeif

et al., 2016a, 2016b, 2018; Radwan et al., 2020c; Mutebi et al., 2021). Polarizing microscopy of thin sections was used for petrographic analysis of the rock samples. The lithological interpretation of the reservoir was based on the study of thin sections that were prepared from core samples. The cores samples cover the depth interval of 11,413–11,488 ft¹ in the July-93 well. These data were integrated to evaluate the Matulla Formation and to delineate its facies distribution. The various lithologies/facies properties were used as input in the created 3D structural system via facies modeling processes to obtain a 3D facies model for the Matulla reservoir.

¹ 1 ft = 0.3048 m.

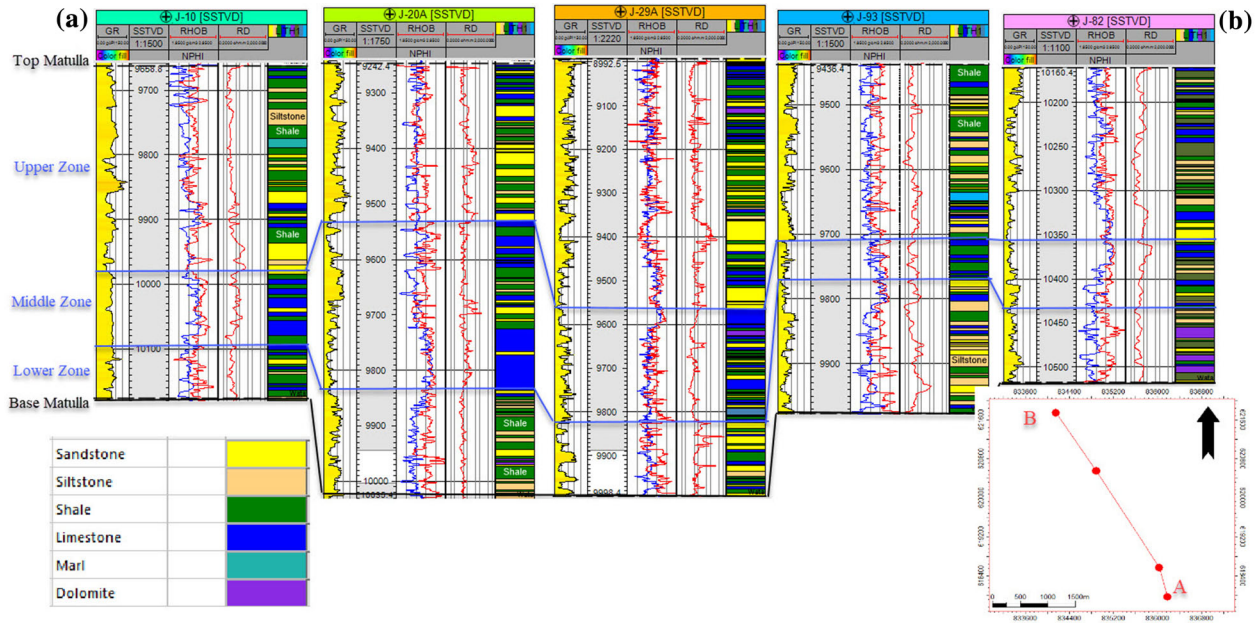


Figure 4. Well correlations across A–B section showing the logs' reaction and the divided zones through the Matulla Formation. The upper zone is predominantly an interbedded sand and shale sequence. The middle zone is predominantly an interbedded carbonate and shale sequence. The lower zone is predominantly an interbedded sand, shale and carbonate sequence. (1 ft = 0.3048 m).

Petrophysical Analysis

The petrophysical evaluation was performed through study of the various well logging curves (Fig. 4). The goal of petrophysical analysis was to determine the key parameters that were needed for reservoir characterization and assessment of hydrocarbon potentiality. In this study, wireline logging, composite logs, and internal geological reports were used to evaluate and delineate the reservoir petrophysical properties. The critical parameters of the Matulla Formation (i.e., effective porosities, shale volume, water and hydrocarbon saturations) were determined using industry standard techniques. The water saturation estimation in the contaminated Matulla sandstone with varied percentage of clays across the reservoir was done using the Indonesian equation of Poupon and Leveaux, (1971). Subtracting S_w from 100 percent saturation yields the hydrocarbon saturation (S_{hc}). Water resistivity (R_w) equals $0.013 \Omega \text{ m}$ according to Pickett plots (i.e., resistivity–porosity relationship).

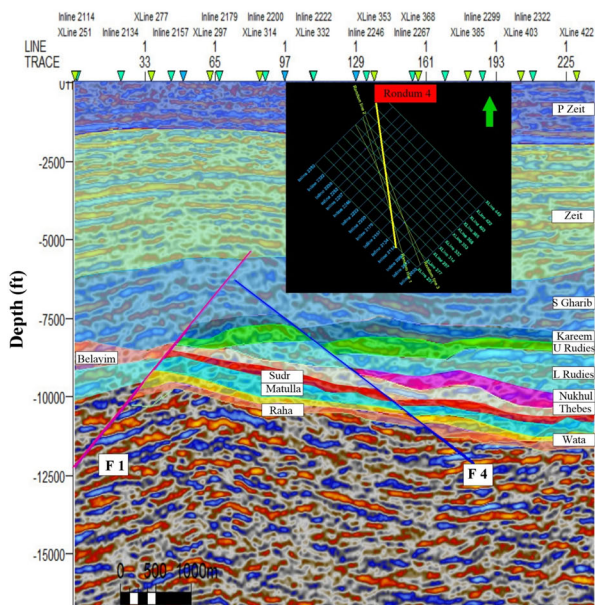
The net reservoir and pay thicknesses were calculated using standard cut-off, where the percentages of porosity, shale volume, and water saturation were 10%, 35%, and 50%, respectively. The

results of the petrophysical analysis were used as inputs into the created 3D structural system via petrophysical modeling to obtain a 3D petrophysical model for the reservoir.

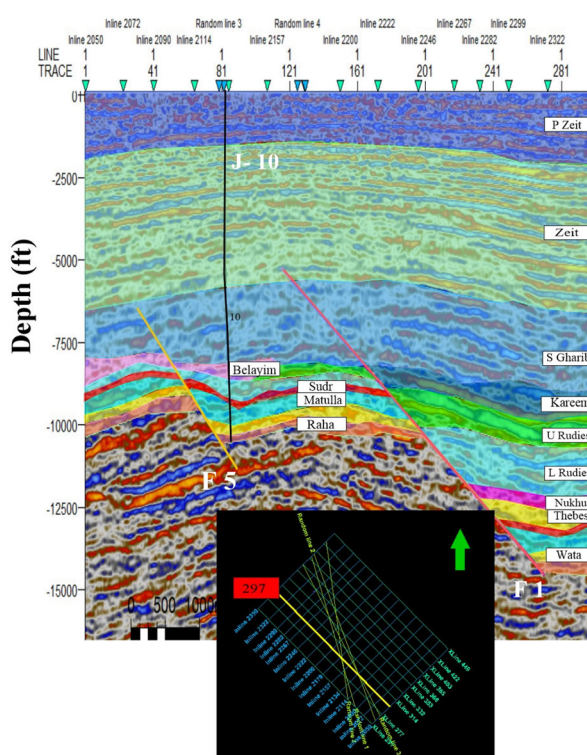
Facies Modeling

The basic goal of reservoir description was to identify reservoir heterogeneities that affect the amount, position, accessibility, and movement of fluids across the reservoir. Because standard data collecting methods produce sparse sampling, 3D description at the appropriate resolution was generally problematic. In order to “predict“ geological, geophysical, and petrophysical properties between sampling points (e.g., wells and seismic lines) and define probable variabilities, geostatistical approaches were used (Radwan, 2022; Seifert & Jensen, 1999).

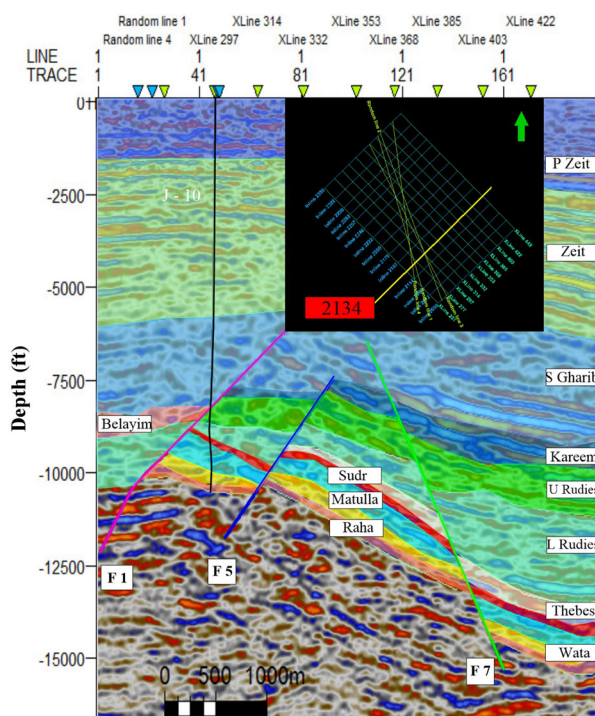
To build the 3D facies model, the allocated values were loaded into Petrel™ software in a distinct code for the lithology distribution, and then dispersed in two directions (vertically and horizontally) across the grid cells to fill the full 3D grid between the wells (Abdel-Fattah et al., 2018; God-



(a)



(b)



(c)

◀ **Figure 5.** Interpreted 2D-seismic lines. (a) Random seismic line 04 along N–S trend. (b) Line 297 passing through July 10 well along NW–SE trend. (c) Line 2134 passing through July-10 well along NE–SW trend.

will & Waburoko, 2016; Jika et al., 2020; Okoli et al., 2021; Radwan, 2022). In addition, the 3D facies model was applied using the stochastic sequential indicator simulation (SIS) method (Deutsch & Journel, 1998; Journel, 1982; Radwan, 2022; Remy et al., 2009). This algorithm is the most widely used for discrete or categorical variable data such as facies, whereby upscaled facies values and allocated variograms are the most important factors (Deutsch & Journel, 1998; Radwan, 2022).

When using stochastic modeling, SIS, a number of uncertainties can arise. In this simulation approach, a grid-node that has no simulated value (an unknown lithotype) is selected randomly and neighboring node points are identified and simulated with reference to the original conditioning dataset.

Later, another grid-node is selected randomly, and the variable is simulated using the newly generated CDF (cumulative distribution function), which is now increased in size by one value. In this way, each node is simulated (Deutsch & Journel, 1998; Seifert & Jensen, 1999; Okoli et al., 202; Radwan, 2022).

Petrophysical Modeling

The main petrophysical parameters models were constructed based on the IPTM software’s interpretation of the results (Cannon, 2018). Because the available data for deterministic modeling were insufficient, a stochastic method was employed instead. Only the vertical well profiles were used as bases for the 3D spreading of the petrophysical properties. For the Matulla reservoir petrophysical parameters, the normal score transformation was used. As a statistical approach that works with the amount of available data, namely the SGS algo-

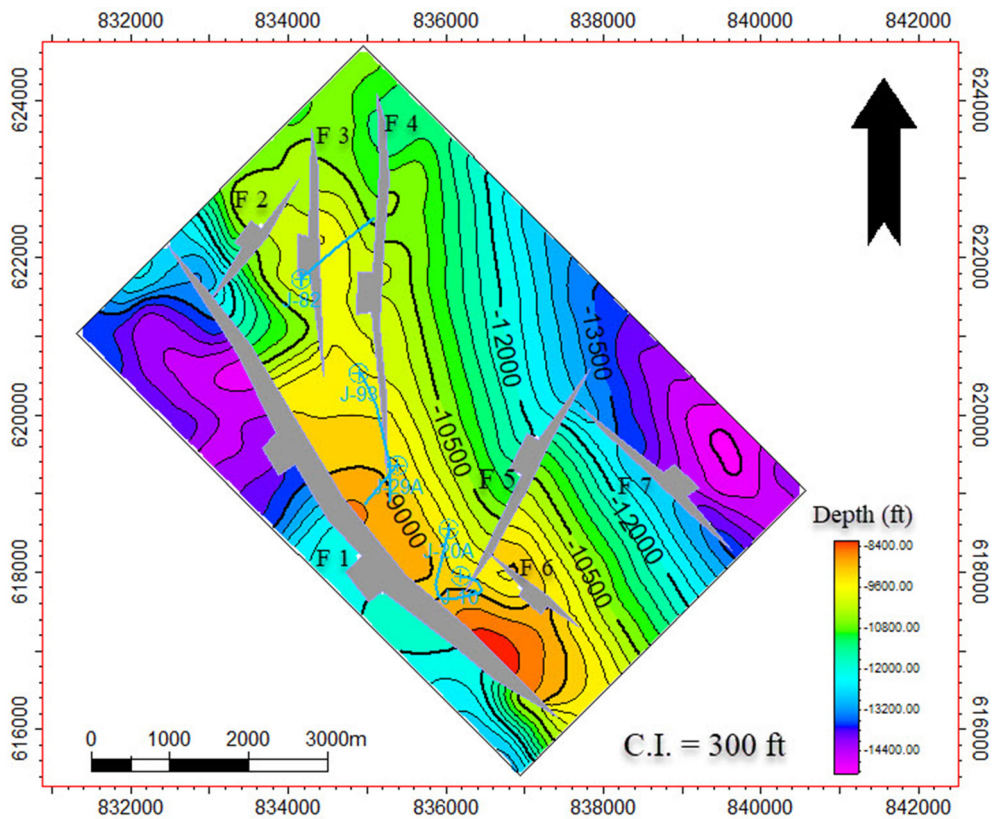


Figure 6. Depth structure contour map of the top of Matulla Formation. X and Y coordinates are connected to the projection of Gulf of Suez, Egypt S-650 TL/Red Belt (1 ft = 0.3048 m).

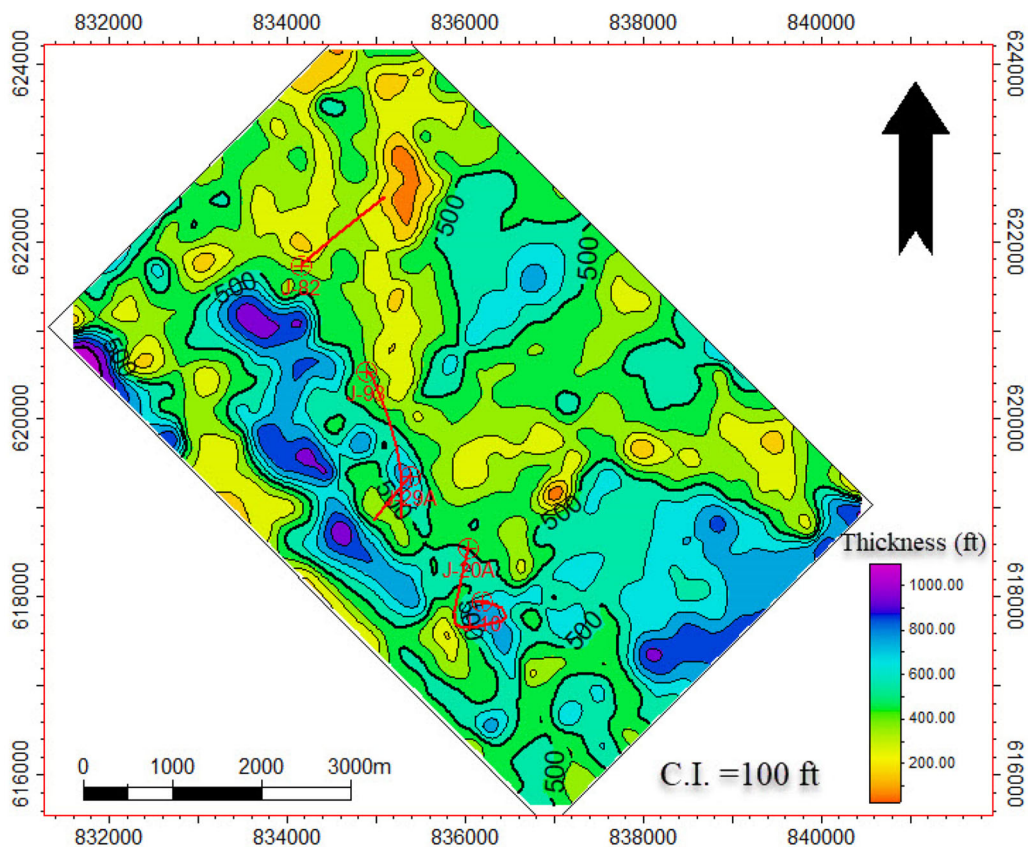


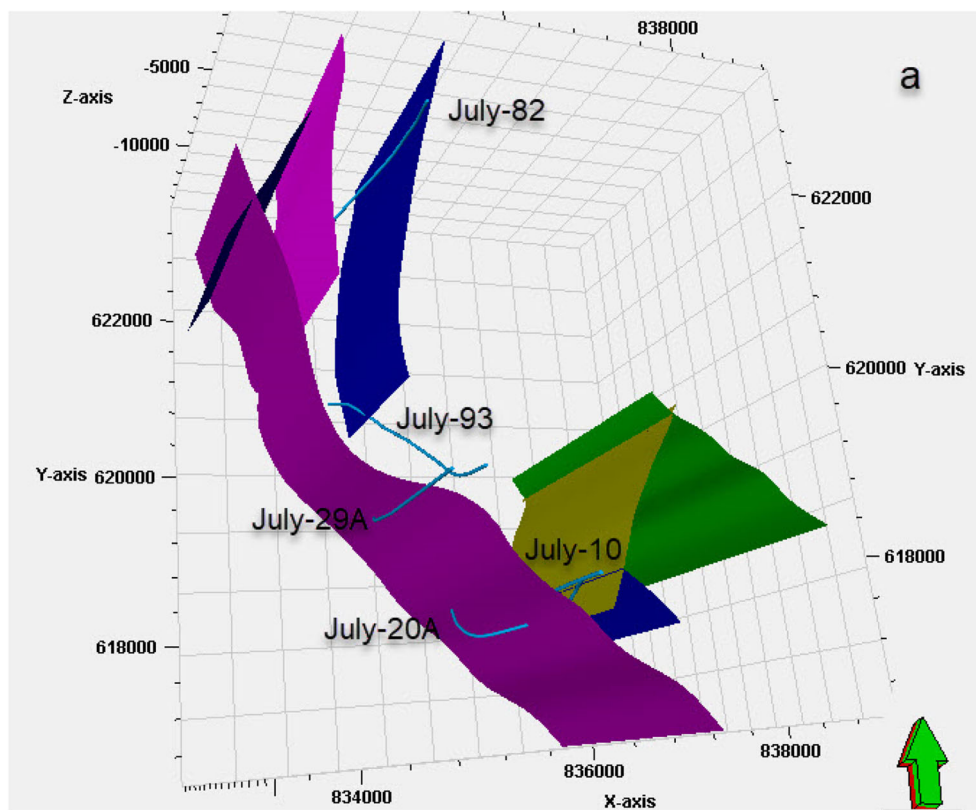
Figure 7. Isopach contour map of the Matulla Formation. X and Y coordinates are the same as in Fig. 6 (1 ft = 0.3048 m).

rithm, was used (Pyrz & Deutsch, 2014; Radwan, 2022). The major inputs for the petrophysical modeling included upscaling of well logs, input distribution, and variogram construction. The vertical range was set to twice the zone’s thickness. To ensure that the transformation applied to the data was reasonable (valid), a statistical quality check was done between both of the upscaled and modeled petrophysical attributes to ensure that the upscaled and modeled petrophysical characteristics’ standard deviations and variances were nearly identical (Abdelmaksoud et al., 2019a; Radwan, 2022).

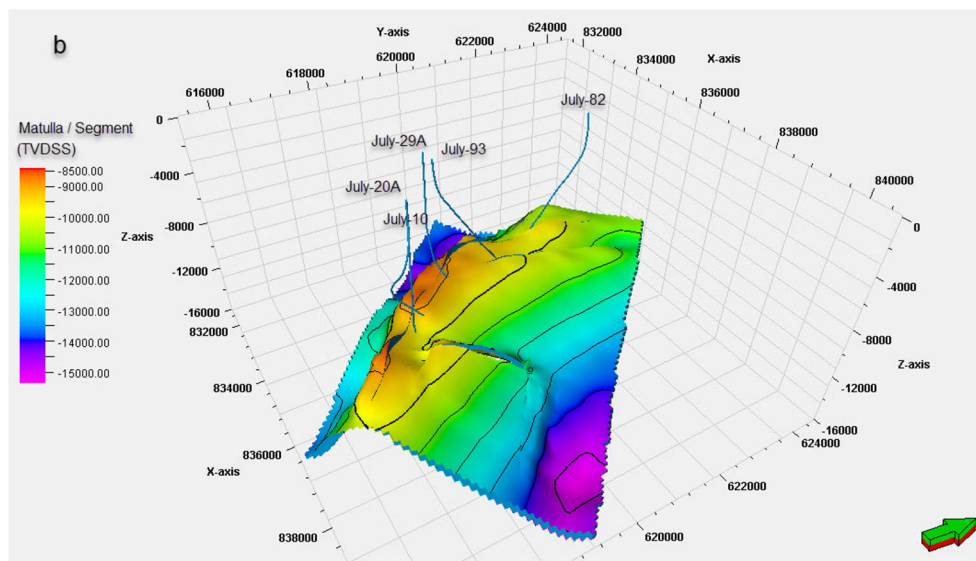
RESULTS AND DISCUSSION

Depth Structure Contour Map of the Matulla Formation

After completing the seismic interpretation process for all lines, the seismic to well tie was performed. The studied horizons were then selected on seismic sections, and the faults affecting them were interpreted (Fig. 5a, b, c). The preceding steps made it simple to create depth structure contour map of the Matulla Formation. The reflection map (Fig. 6) at the top of the Matulla Formation shows strong spatial variability of the horizon in the study area, with a general deepening to the southeast and northwest reaching maximum value of $-15,000$ ft TVD_{SS} (true vertical depth subsea), at seismic shotpoint (S.P.) 181 on seismic line 2072. In addition, the seismic line 2134 at S.P. 41 showed topog-



(a)



(b)

Figure 8. (a) Final adjusted faults in the fault model of the study area. Different colors indicate various faults. (b) 3D view of the modeled Matulla horizon displaced by faults.

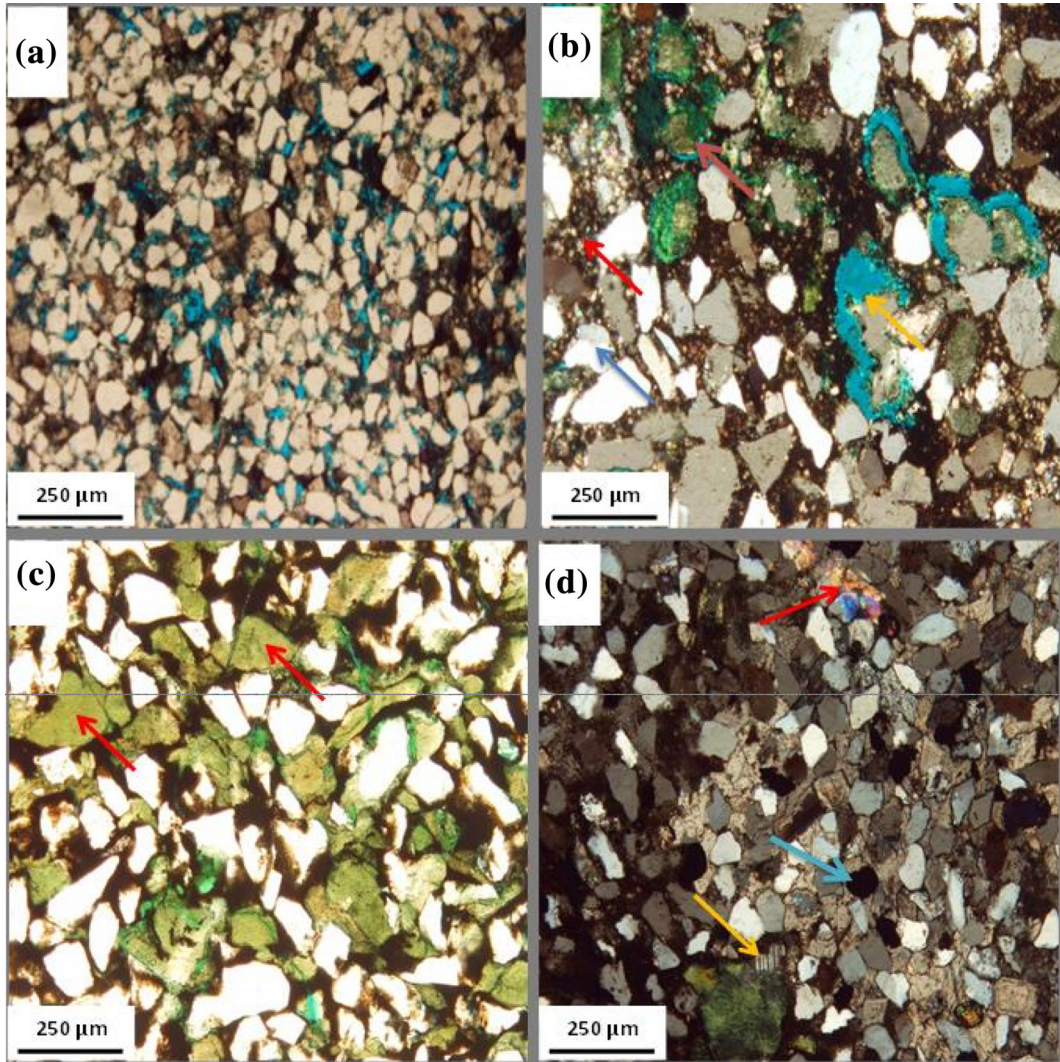


Figure 9. (a) Variable grain sizes in moderately sorted sublithic arenite, plane polarized light: magnification 40 ×, at 11,431 and 11,433 ft depth. (b) Moderately sorted quartz grains agglutinated by (glauconitic dolomitic sublithic arenite), orange arrows point to secondary pores where carbonate framework grains were dissolved. Blue arrows point to orthoclase grains, red arrows points to rhombs dolomite and brown arrows points to glauconite, at 11,444 ft depth. (c) Fine size quartz grains with numerous glauconitic pellets (ferruginous glauconitic greensands). Red arrows point to glauconitic grains, at 11,447 ft depth. (d) Highlight calcite cementation. Red arrow points to high interference colors of a mica flack, light blue arrow points to heavy minerals with quartz grains, orange arrow points to plagioclase grain, at 11,449 ft depth. (1 ft = 0.3048 m).

raphy shallowing to the west and southwest sections of the region, with minimum value of -8200 ft TVD_{SS}. The main faults delineated on seismic sections showed a clear NW–SE-trending fault (Red Sea System), which primarily dips southwest with some faults in the southern part dipping northeast and forming horsts. The other major NE–SW and N–S faults are thrown northwestward. As shown in Figure 5, the Matulla Formation structures contain

faults and horsts structural closures, which were also noticeable in the majority of the study area.

Isopach Map of the Matulla Formation

The Matulla Formation reservoir’s isopach map was created by subtracting the Wata interval’s depth map from the Matulla interval’s depth map (see

Table 1. Summary of derived petrophysical parameters of the Matulla Formation.

Well name	Gross interval (ft*)	Net pay (ft)	Effective porosity (%)	Water saturation (SW %)	Shale volume (Vsh %)	Hydrocarbon saturation (Shc %)
July—10	534	110	16	18	12	82
July—20A	1095	300	15	21	14	79
July—29A	1334	250	17	15	13	85
July—82	384	80	13	32	18	68
July—93	584	175	16	24	17	76

*1 ft = 0.3048 m

stratigraphic position in Fig. 2). All of the wells investigated (July-10, July-20A, July-29A, July-82, and July-93) penetrated the Matulla Formation in this region. The Matulla Formation isopach map (Fig. 7) shows that the thickness of the Matulla Formation increases in the southeast and west sections of the July oilfield. However, the thickness decreases in the central and north eastern sections of the July oilfield. The basinal area is directed to the southeast and west parts of the July oilfield and has a maximum thickness of 1100 ft, while the central and northeast parts of the July oilfield are on the platform and have minimum thickness of less than 100 ft.

3D Structural Model

A precise structural model of the Matulla Formation was required for the explanation and knowledge of the structural pattern of the reservoir in a 3D outline. By optimizing the information from seismic data, the goal was to create a solid structural model using the available wells (Fig. 8). The July oilfield is a highly faulted, complex system that generates 46 fault blocks from four reservoirs (Day & Hoffman, 1997), some of which are isolated and have different fluid properties as well as performance and depletion characteristics (Baack & Latif, 1995). The 3D structural framework illustrates complex structures that affect the July area, with normal faulting serving as the primary faulting system. According to the 3D structural model, normal faults with NW–SE trends represent the dominant fault system in the July oilfield. At the uppermost sandstone of the Matulla Formation, the crest of the structure occurs at ~ 9000 ft TVD_{SS} in the central area of the main part of the oilfield (present study), whereas the OWC is at $-10,800$ ft TVD_{SS}, giving an oil column of ~ 500 ft (Marttila & El Bahr, 1994). Moreover, the model indicated that the horizon

depths of the Matulla Formation reservoir were greatest in the eastern and southern east parts of the July oilfield and decreased gradually toward the center and margins of the basin.

Petrographic Analysis and Lithological Features

Evaluation of sedimentological and well log analysis is the key for better reservoir discrimination and better reservoir quality prediction (Radwan, 2021a; Radwan et al., 2021c; Qadri et al., 2021). The Matulla Formation petrographic studies and micro-facies analysis were carried out on samples from well July-93, based on the cumulative core interval from 11,413 ft to 11,488 ft (75 ft of total thickness). The stratigraphic section of the Matulla reservoir was composed of fine- to very fine-grained clastic sediments, according to thin section sample analysis, core samples, and well logging analysis. The dominant lithologies were sandstones, shales and limestones accompanied by minor siltstone. The Matulla shale had a dark gray color, and the shale cuttings had moderate hardness and sub-blocky shape. Moreover, the Matulla shales were non-calcareous to slightly calcareous. In terms of hardness and crystallinity, the Matulla limestones were moderately hard and cryptocrystalline. The Matulla limestones were, in contrast, highly argillaceous, indicating the origin of these limestones gray colors. The petrographic characterization of the Matulla sandstones is discussed below (Fig. 9).

Grain Framework

According to thin section analysis, quartz grains were the most abundant mineral constituents of the Matulla sandstone, accounting for more than 70% of the individual samples. Many samples contained monocrystalline and polycrystalline quartz grains.

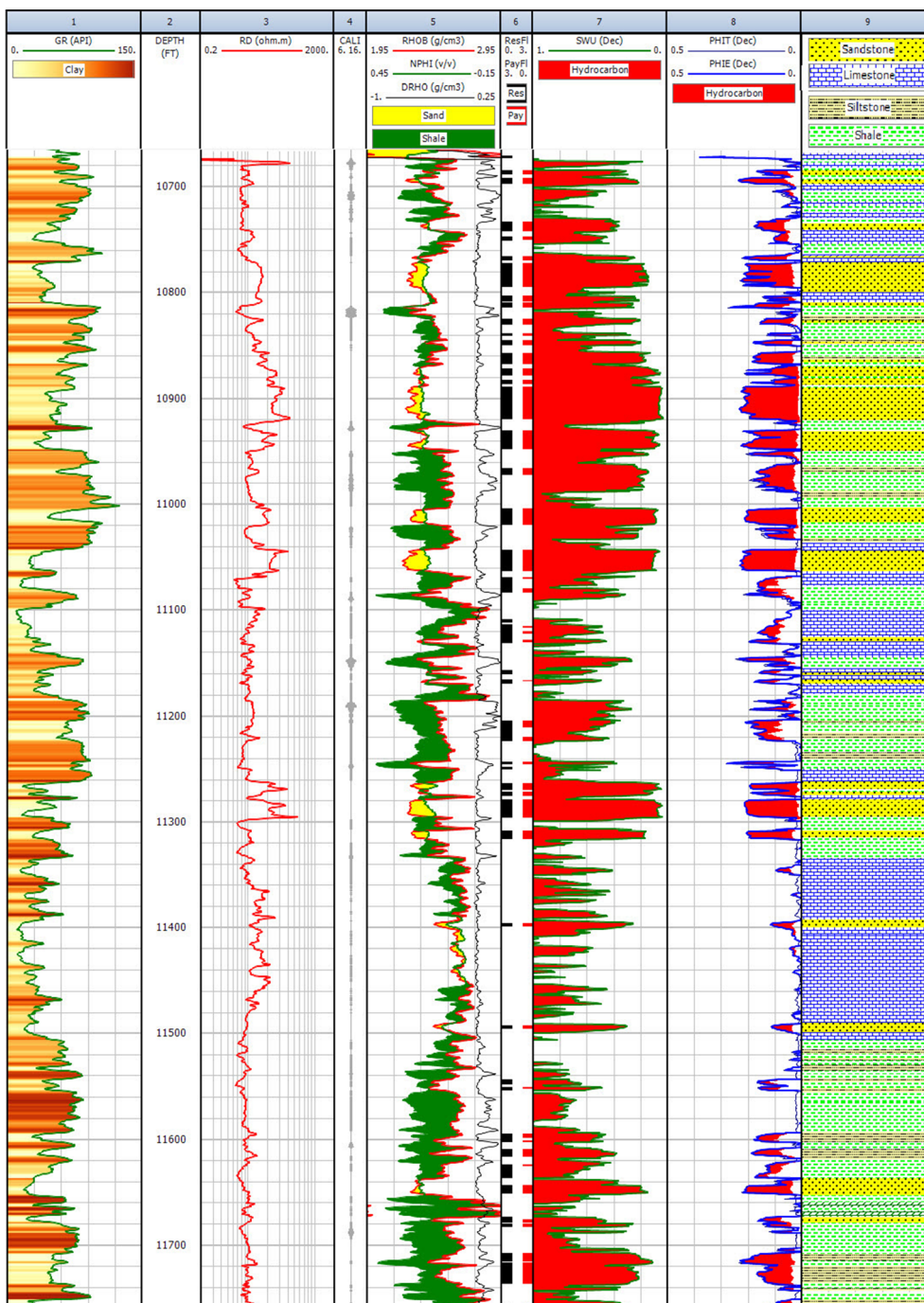


Figure 10. Litho-saturation cross-plots of the Matulla reservoir (July 20A well) (1 ft = 0.3048 m).

Lithic fragments were the second most common constituents of Matulla sandstones, comprising about 10%. Feldspars were the less abundant constituents of Matulla sandstones with variable degrees of alteration found in the majority of samples, with

orthoclase accounting for about 5% of the feldspar grains. Accessory minerals averaged between 1 and 2%, and included glauconite, zircon, pyrite and mica. Glauconite may reach a higher percentage in some samples, forming green sandstone in this case.

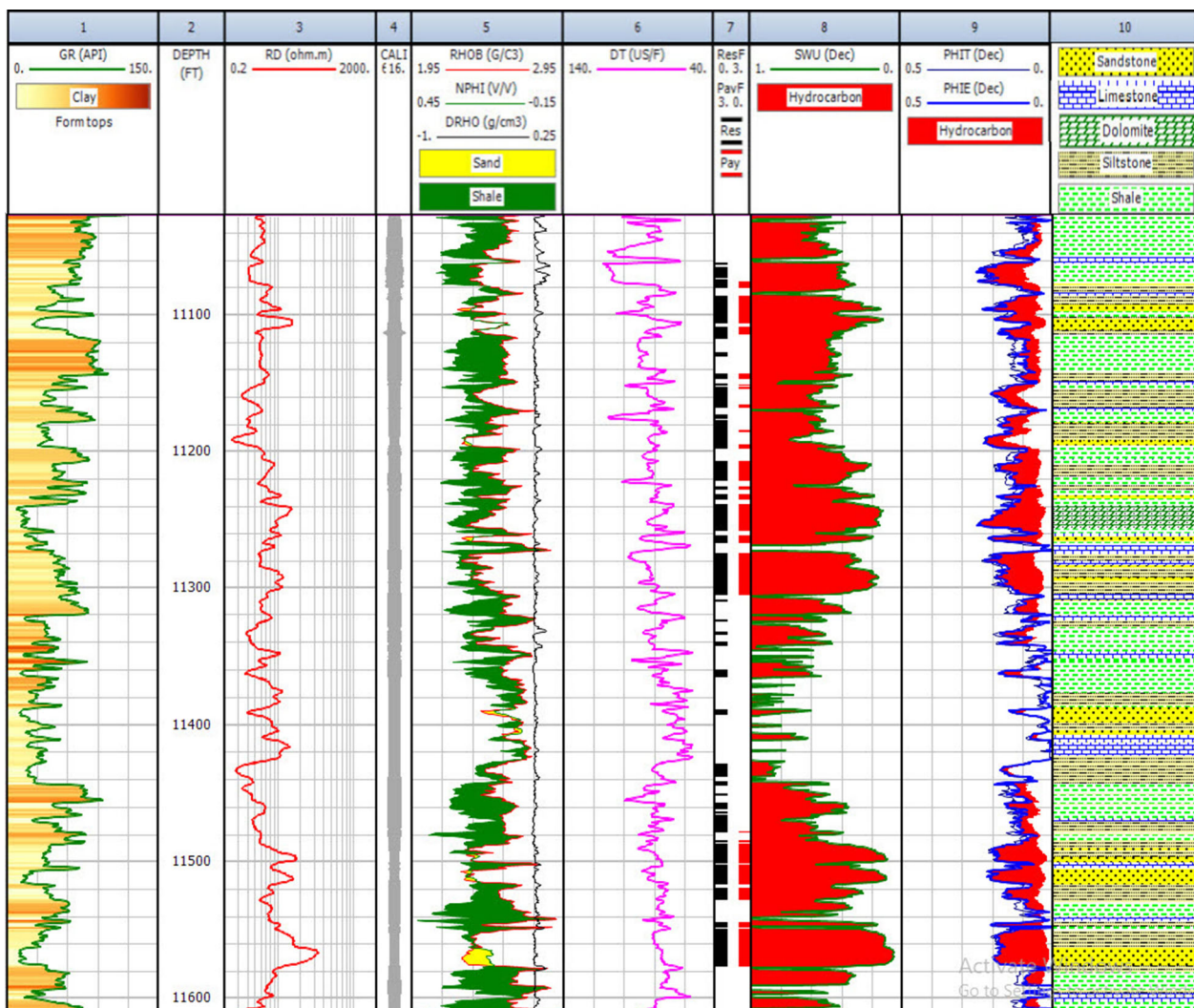


Figure 11. Litho-saturation cross-plots of the Matulla reservoir (July 93 well) (1 ft = 0.3048 m).

According to the sandstone classification, the Matulla sandstone can be classified sub-lithic arenite sandstone (Pettijohn & Potter, 2012). Variable porosities, primarily of the inter-particle and intra-particle types, were found between the grains, limiting the ability of the reservoir to store oil.

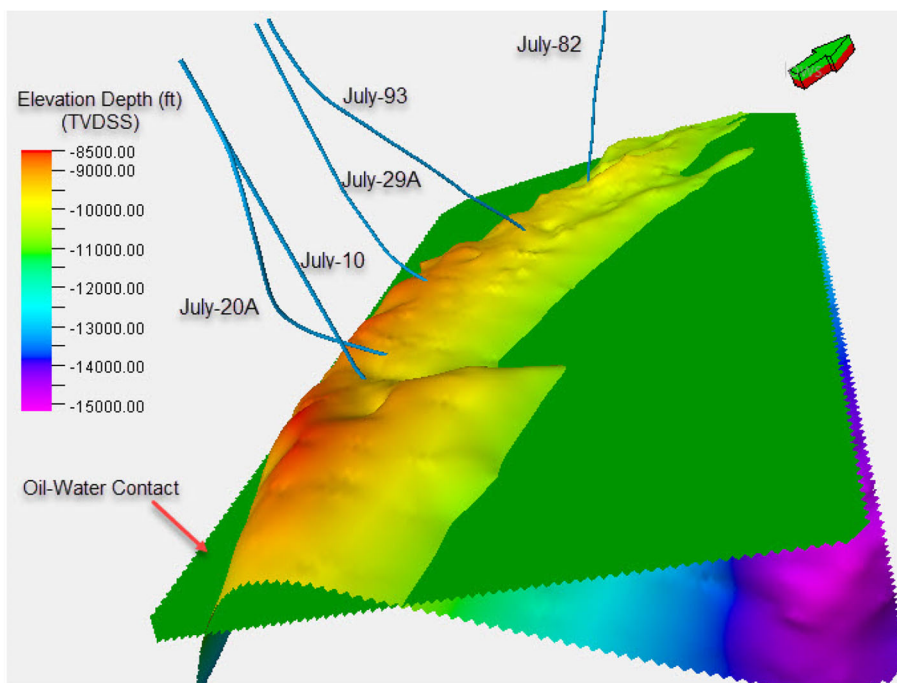
Cement and Matrix

The upper part of the core interval was cemented with calcite, dolomite rhombs, and glauconitic grains, while the lower part was cemented with argillaceous, dolomite, and glauconitic materi-

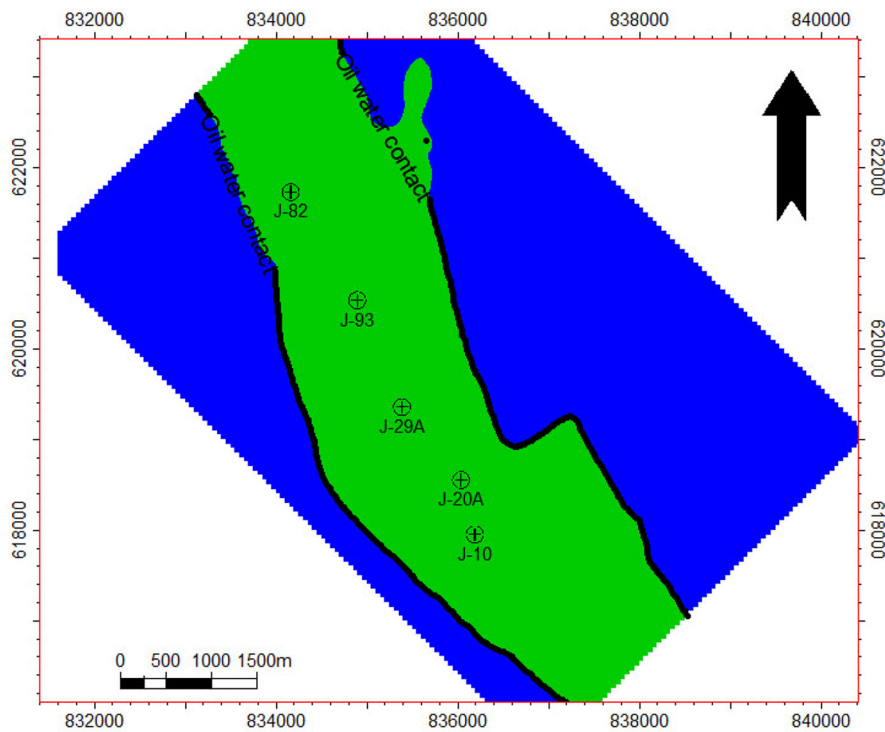
als. However, silica cement is uncommon. Silt-size matrix is dominant in the Matulla reservoir.

Texture and Fabric

Quartz grains were sub-angular to sub-rounded, with the latter being more prevalent in the succession. The Matulla sandstone reservoirs in the July field had grain sizes ranging from fine to very fine sand. In most samples, the well sorted texture was dominant; however, some samples were moderately sorted.



(a)



(b)

Figure 12. Hydrocarbon distribution model: (a) oil water contact trace in July oilfield; (b) 2D map view displaying well locations in the oil zone.

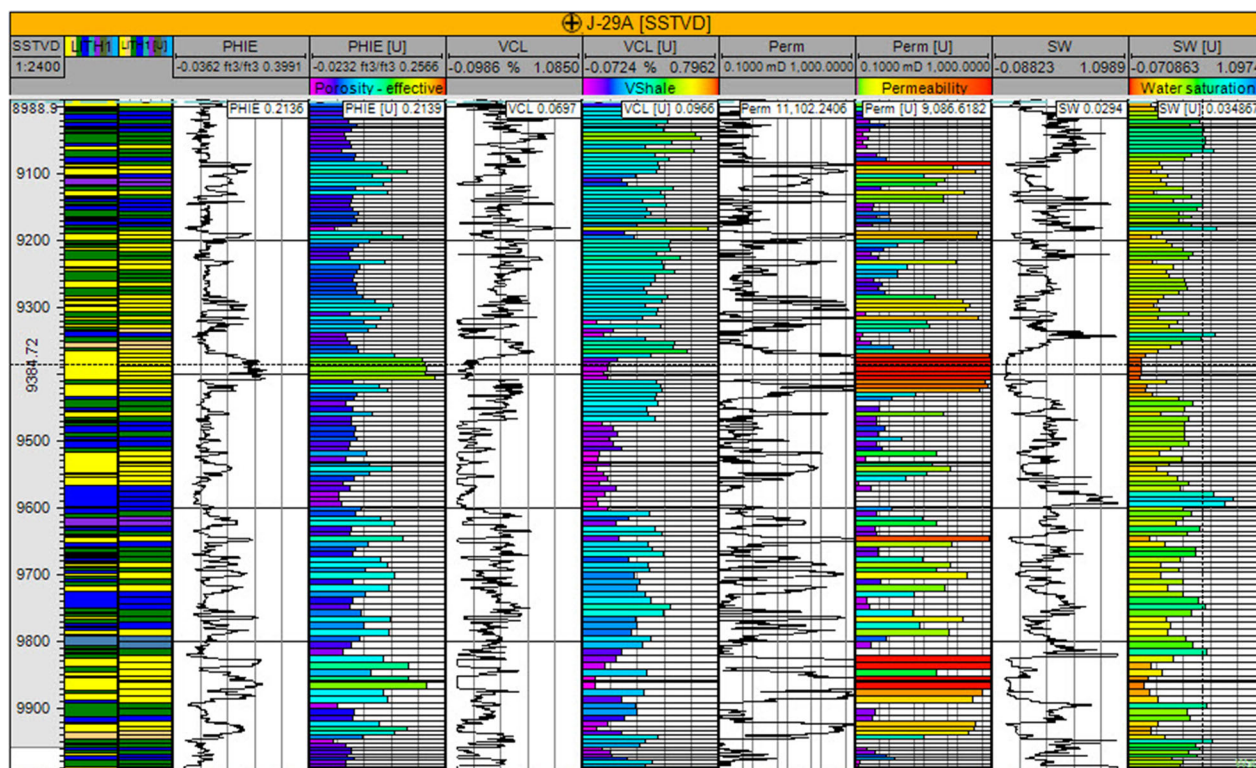


Figure 13. Quality control of the upscaled (discrete) facies and (continuous) petrophysical properties logs for July (29A) well.

Diagenetic Features

Many processes have reduced the reservoir potential of different facies types, according to diagenesis studies of the Matulla sandstones. In decreasing order of importance, detrital clays, carbonate cementation (calcite and dolomite), compaction, and kaolinite formation were observed. The pore system and reservoir potential both increased due to two factors occurring during diagenesis: dissolution and fracturing. Some of the samples exhibited minor dissolution of detrital grains (primarily feldspars) and partial dissolution of carbonate cements and clays.

Petrophysical Parameters of the Matulla Formation

The petrophysical and hydrocarbon characteristics of the Matulla Formation were based mainly on well logging analysis of the five studied wells, which were distributed across the study area. The average values of the various derived petrophysical parameters of the examined wells of the July oilfield

are summarized in Table 1. The petrophysical data logs of selected wells from the July oilfield are depicted in Figures 10 and 11.

The Matulla Formation in the July oilfield was encountered in the depth range 9766–10,300 ft in July 10, 10,665–11,760 ft in July 20A, 9350–10,690 ft in July 29A, 11,086–11,462 ft in July 82, and 11,027–11,611 ft in July 93. The lateral and vertical changes in petrophysical properties were thought to be directly connected to lateral and vertical facies changes across the Matulla reservoir. The petrophysical analyses of the wells under consideration showed good reservoir properties and hydrocarbon fluid entrapment in the Matulla Formation. The litho-saturation cross-plot revealed a complex lithologic nature that varied between sandstone, carbonate and shale with silt intercalations at different levels. Relatively low GR, high resistivity, high density, and low neutron porosity logs were recorded against carbonate lithology intercalated with shale zones. Along the shale zones, high GR, low resistivity, low density, and high neutron porosity values were observed. However, the sandstone had low gamma ray readings, porosity ranging from low to intermediate,

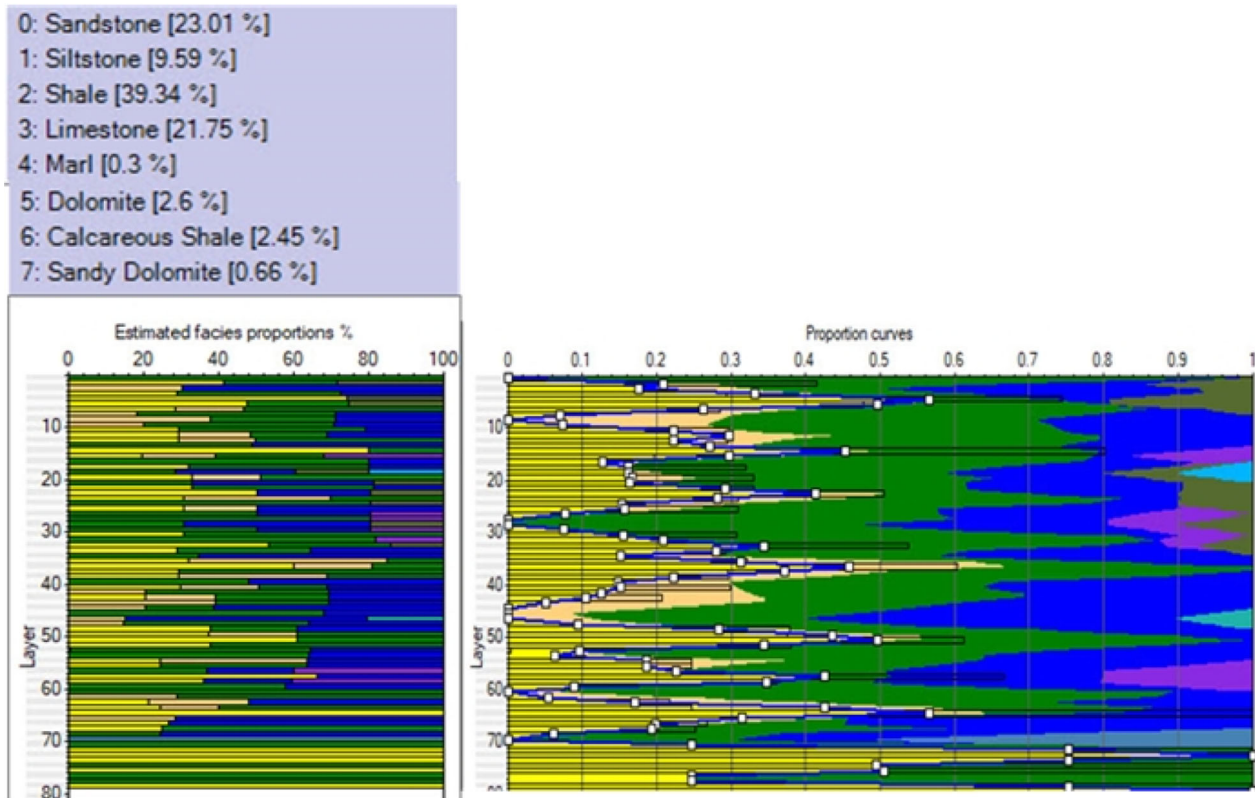


Figure 14. Facies proportions vs. layers of the Matulla Formation.

and bulk density was moderate, whereas deep resistivity varied with fluid content (2–200 Ω-m).

To distinguish the entire Matulla Formation, it was divided into three zones: upper, middle, and lower (see well correlations in Fig. 4). Pore fluid discrimination is critical in petrophysical evaluation (Agbasi et al., 2018; Radwan et al., 2020c). Oil was the fluid type in the Matulla Formation, and the majority of the source rocks in the July oilfield were oil prone (EGPC, 1996; Day & Hoffman, 1997). Figure 12a and 12b display the oil water contact at depth of – 10,600 ft TVD_{SS}, providing a large column of oil in the Matulla reservoir. According to the petrophysical investigation, the Matulla sandstone had excellent reservoir characteristics and that it can store and transfer hydrocarbons. The statistical analyses showed a good range of total and effective porosity, as well as permeability, implying that the Matulla Formation’s reservoir quality was good. The extreme lateral and vertical changes in lithology may be linked to the significant lateral and vertical changes in petrophysical properties of the Matulla reservoir.

3D Facies Model

The initial stage in facies modeling is to create discrete facies that are upscaled (Fig. 13) to grid-based model cells (Abd El-Gawad et al., 2019; Radwan, 2022; Tyson, 2007). In terms of lithology, the Matulla Formation displayed various lithologies due to the facies changes from sandstone and shales to carbonate facies. In comparison to sandstone, the shale fraction had a larger proportion of the probability distribution, followed by limestone and siltstone in decreasing order of abundance. The outcomes of the data analysis were employed for facies modeling. Based on the combined sedimentological and petrophysical analysis, the following were the proportions of the various lithologies used: 23% sandstone, 9.6% siltstone, 39.3% shale, 21.7% limestone, 3.8% calcareous shale, and 2.6% dolomite (Fig.14). The interpreted facies of mixed carbonate/siliciclastic facies of the Matulla Formation consisted of different lithologies that have been deposited from lower intertidal to slightly deep subtidal in a fluctuating depositional regime. El-Azabi

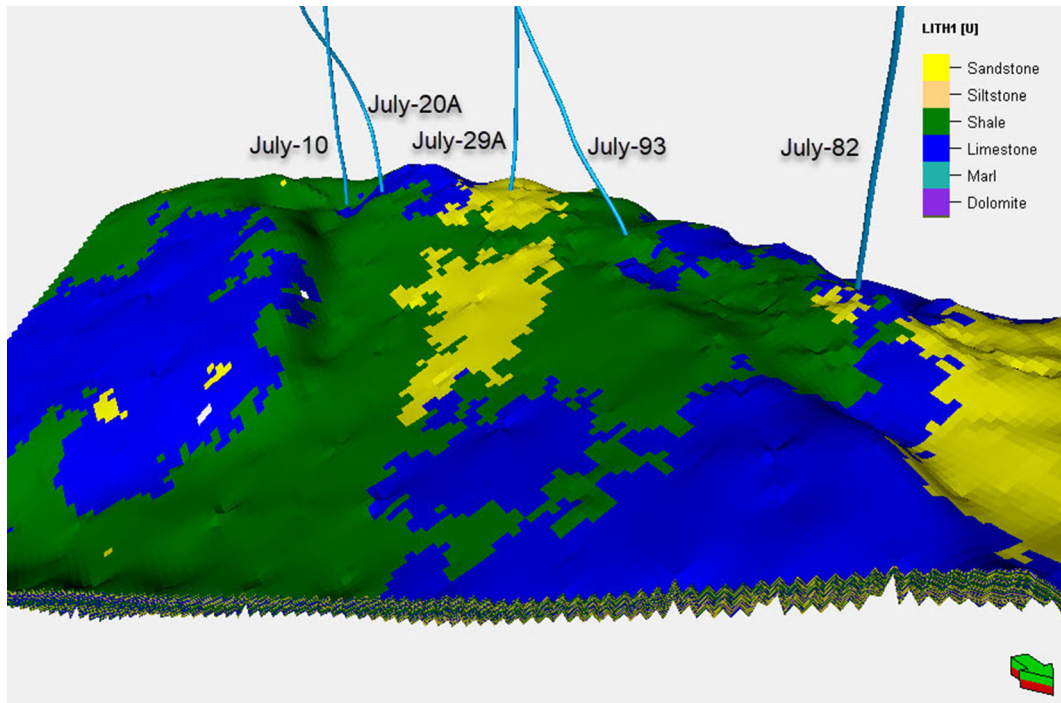


Figure 15. Static model showing top view of the facies model of the Matulla Formation. The X- and Y-axes are measured in meters, whereas the Z-axis is measured in feet (1 ft. = 0.3048 m).

and El-Araby (2007) interpreted various types of foreshore sandstone environments and shallow subtidal siltstone for the Matulla Formation; however, they also described deep subtidal shale/claystone and shallow water lime-mudstone. Cross sections of the Matulla Formation reservoir were generated in addition to the facies model (Fig. 15) to highlight the lateral and vertical facies changes (Fig. 16). Facies variation from continental fluvial to marine facies with tidal flood plain conditions in between reflects sea level fluctuations through the Matulla Formation (El-Azabi & El-Araby, 2007). The rapid facies changes across the studied wells reflect the changes in depositional conditions.

3D Petrophysical Model

The interpreted petrophysical characteristics of the Interactive Petrophysics Program were upscaled and then modeled using standard procedures. In the process of petrophysical modeling, the SGS algorithm was the utilized statistical approach (Ali et al., 2019a, 2019b; Radwan, 2022). Given the amount of available data, this approach is most likely the best

fit in this case, where it had the advantages of simulating continuous variables such as permeability and porosity (data after being normalized) (Fig. 14). The parameter values of unsampled intervals were determined using the equations derived from data regression during SGS, and then all values were forced to satisfy the normal distribution by normal scoring. The fundamental simulation parameters are illustrated in Figure 17. In order to characterize the 3D distribution of these specific attributes within the July oilfield, several cross sections were derived from these models (Fig. 18).

The petrophysical model of the Matulla reservoir upper zone showed high to intermediate porosity and permeability values that generally increased in the central and southwest directions. The upper part of the Matulla reservoir in the studied region had relatively intermediate water saturation values, and shale volume decreased in the central and southwest directions. Low effective porosity values, on the other hand, were observed in the middle zone, particularly in the north and south of the area. Permeability values in this zone were also low, with general increase in the study area's central and southeast sectors. In addition, the model showed

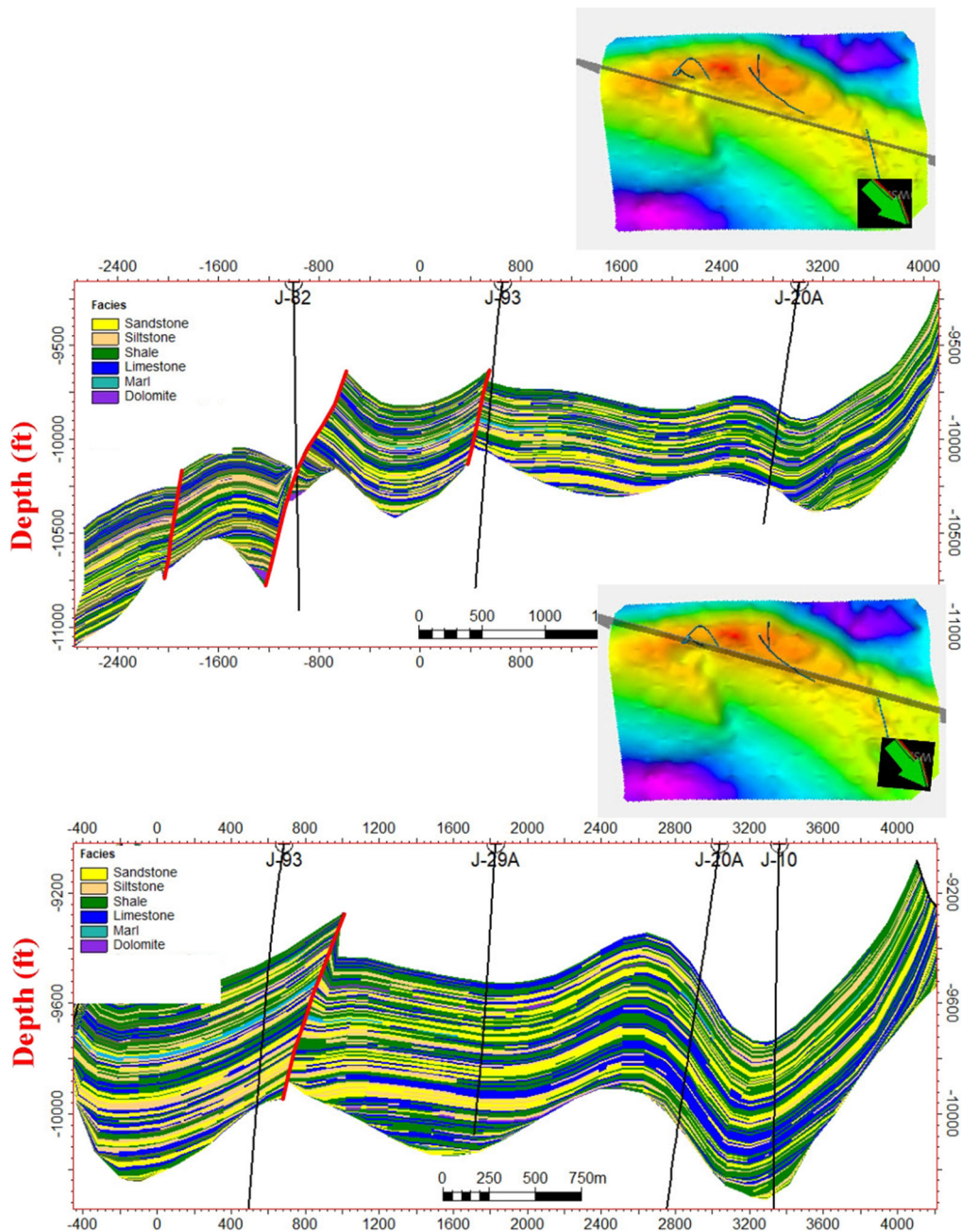


Figure 16. Cross sections showing the facies model of the Matulla Formation. The X- and Y-axes are measured in meters, whereas the Z-axis is measured in feet (1 ft. = 0.3048 m).

relatively high values of water saturation and shale volume, which were decreasing in the central and southeast sectors. These results explain the increase in effective porosity and permeability in the lower zone, with slight increase in the north and central

directions. This lower zone had relatively low water saturation and shale volume.

We deduced that the upper zone had overall good to very good reservoir quality (high porosity, low shale volume, and low water saturations), especially in the middle interval; also, the lower zone

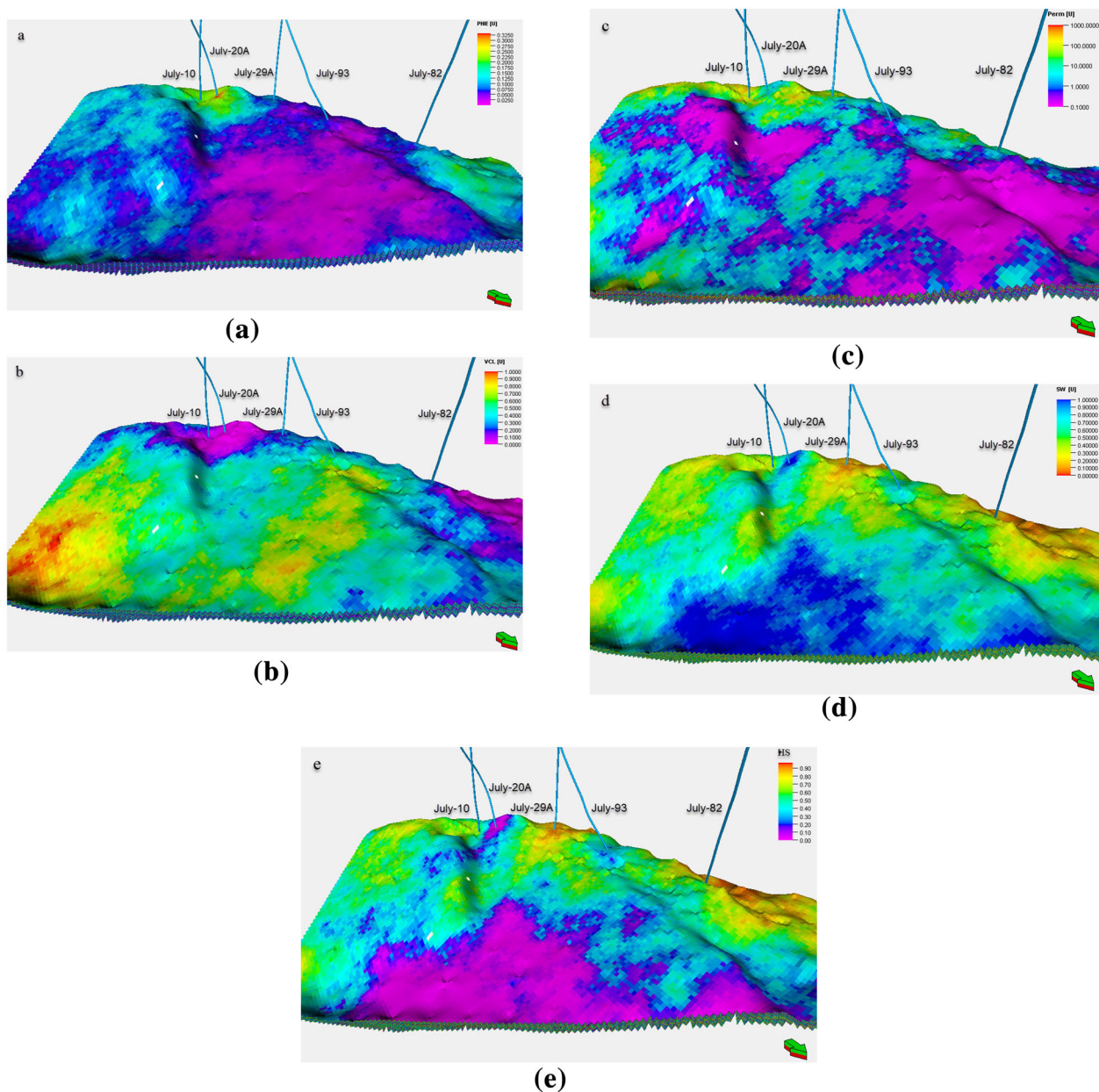


Figure 17. Matulla reservoir static model showing the top view of petrophysical parameters: (a) porosity; (b) shale volume; (c) permeability; (d) water; (e) hydrocarbon saturation. The X- and Y-axes are measured in meters, whereas the Z-axis is measured in feet (1 ft. = 0.3048 m).

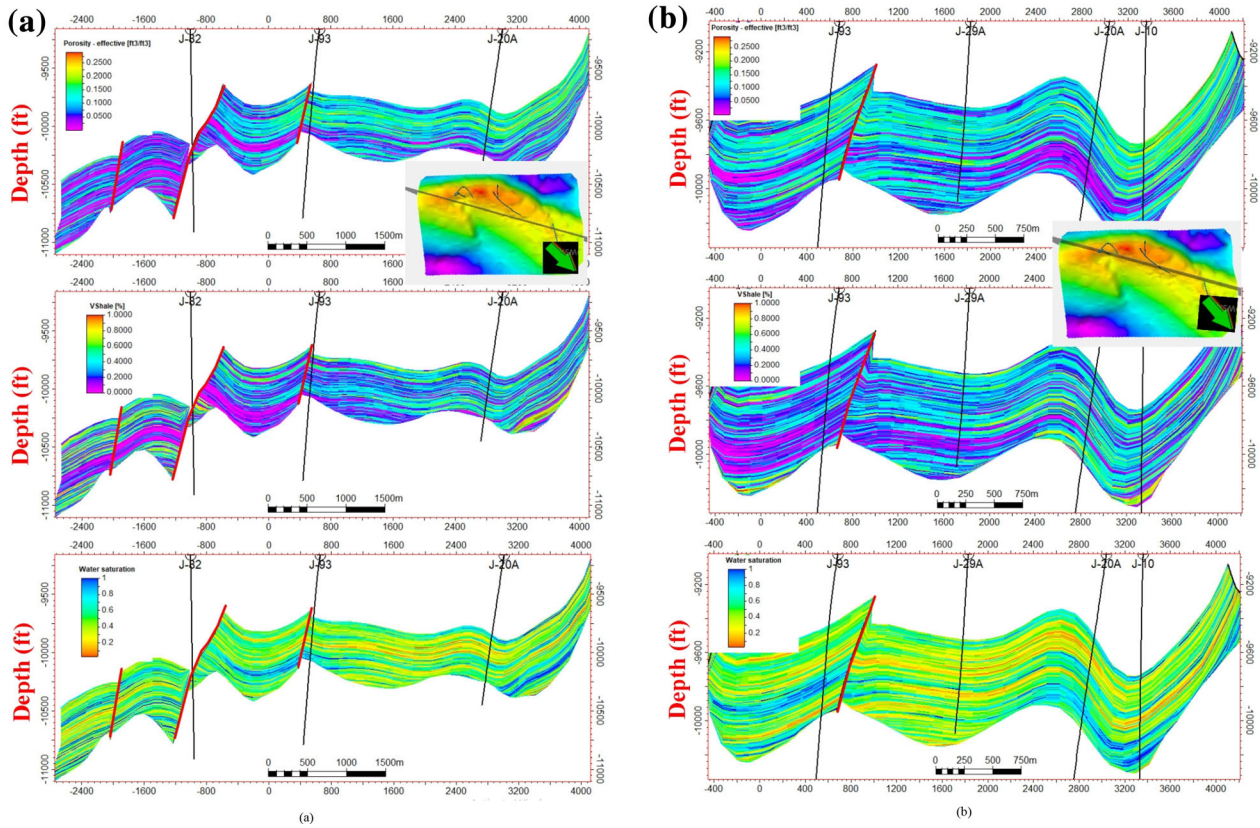


Figure 18. Two cross sections showing the distribution of petrophysical models in NW-SE direction. The X- and Y-axes are measured in meters, whereas the Z-axis is measured in feet (1 ft. = 0.3048 m).

Table 2. Volumetric estimations of Matulla reservoir.

Reservoir	Volume × 10 ⁶ (MCF*)			(OIP) (MSTB**)
	Bulk	Net	Pore	
Matulla	279,842	75,000	1000	715

MCF, million cubic feet; MSTB, million stock tank barrel.

*1 ft³ = 0.0283 m³.

**1 barrel = 0.0158 m³.

was of good quality reservoir. However, the middle zone had poor reservoir quality (low porosity, high shale volume, and high water saturations). Finally, according to the integrated 3d model, the most favorable sectors for hydrocarbon accumulation and production through the Matulla reservoir were located in the central, southeast, and southwest sectors of the July oilfield. Therefore, it is recommended that future development activities be concentrated on these areas.

Volumetric Calculations

For a realistic resource estimation, volumetric calculations were employed in conjunction with geological reservoir models (Attia et al., 2015; Cannon, 2018; El Khadragy et al., 2017; Radwan et al., 2021c, 2022). We used the following formula to compute the volume of hydrocarbons (Dean, 2008):

$$OOIP(STB) = \frac{7758 * a * h * \phi(1 - SW)}{Bo}$$

where *OOIP* is original oil in place, *A* is study area in acres, *h* is net pay thickness in feet, *φ* is porosity in %, *SW* is water saturation in % and *Bo* is the oil formation volume factor. The volumetric estimations of oil within the Matulla reservoir were performed using a 3D grid-based geocellular model developed in this work (Table 2). The *OIP* at the July oilfield was assessed to be 715 million stock tank barrels (MSTB).

Model Uncertainties

Deriving of rock and petrophysical parameters from well logs and cores requires some caution (Radwan et al., 2020c). As with all geological interpretation processes in the energy sector, there are uncertainties that can accompany geological, seismic, and petrophysical interpretations. Uncertainties in interpretation have an impact on resource evaluation and modeling. Uncertainties plague reservoir modeling frequently due to restricted data availability, data quality, difficulty of reservoir design in predicting flow in a specific reservoir, and modeling process uncertainties (Radwan, 2022; Singh et al., 2009). Therefore, it is critical to examine the input data for quality, quantity, and complexities at various scales, as well as to revisit basic assumptions of a modeling workflow's appropriateness in the light of static reservoir uncertainties.

Moreover, the software required integrated resources in order to reposition the base case model with a reasonable degree of certainty for more accurate project assessment, risk analysis, and decision-making. Certain techniques have recently been developed to solve these issues. While great progress has been made in the areas of gridding and upscaling in recent years, significant practical obstacles in reservoir modeling still remain. In the not-too-distant future, effective and accurate depiction of reservoir shape and heterogeneity will come first on the list. This is because, as technology improves, the amount of data acquired from producing oilfields grows, geology understanding improves, and reservoir descriptions are becoming more detailed. Therefore, achieving a balance between explicit representation of reservoir geometry and heterogeneity by gridding and correct capture of their impacts on multi-phase flows via upscaling is often an ongoing challenge in reservoir modeling.

We attempted to perform precise interpretations and extract the best fit input parameters in this work in order to achieve a more precise static model for the Matulla Formation in the July oilfield. Determination, organization, and applications of structural uncertainty describe the key sources of uncertainty in determining seismic quality and its restrictions for improved reservoir characterization. General geologic expertise, regional geology, and some previous work skill from neighboring oilfields were used to fill in the gaps. The reservoir geological information and restricted data are the key sources of uncertainty in lithofacies modeling. As a result,

the spatial distribution of facies or flow units within the three-dimensional structural system is highly uncertain. In this work, we tried to reduce uncertainties in the facies model; therefore, we applied integrated facies analysis, petrographic description, and well logging interpretation across the studied wells. To achieve the best lithofacies interpretation along the whole area, we used SIS.

By using calibrated well-log data and core measurements, the petrophysical models were simulated to estimate the level of uncertainty in the petrophysical parameter distribution. Stochastic modeling is the process of creating synthetic geologic architectures and/or petrophysical property distributions based on quantitative and qualitative data. The availability of core data from the entire Matulla Formation allows for precise determination of the petrophysical parameters as critical input parameters. Volumetrics are derived from a number of reservoir factors that are often interpreted or predicted based on limited data and were subject to uncertainty. Bulk, pore, hydrocarbon pore volume, and *OIIIP* are volumetric measurements used in a hydrocarbon resource appraisal. Uncertainty studies of these volumetric variables necessitate a thorough examination of data uncertainties in associated input variables as well as implication uncertainties when covering restricted data over the entire oilfield. In this work, we used the most likely fit parameters, which were calibrated using core data and production data. We provided a summary of reservoir modeling issues, focusing on the complex geometry of the complex Matulla reservoir and diverse reservoir parameters based on the available data and the most likely extracted reservoir parameters. Adding more data from more exploratory and development wells targeting the Matulla reservoir can result in more refined and highly accurate reservoir models that accurately represent the subsurface Matulla reservoir.

CONCLUSIONS

The present work dealt mainly with the interpretation of geological and geophysical data to evaluate the structure, lithofacies and petrophysical characters as well as the volumetric parameters of the Matulla reservoir and their 3D distribution in the July oilfield. In this study, we used integrated datasets to assess the distribution and quality of the complex Matulla reservoir, as well as to reduce

uncertainty during oilfield development in July. The following were the main findings of this study.

- The contour lines of depth-structure contour maps showed the spatial variability of the top and base of the Matulla reservoir across the July oilfield with a general deep topography to the southeast and northwest reaching maximum value of 15,000 ft. However, the Matulla contour lines displayed shallow topography to the west and southwest sections of the region, which was mapped to minimum value of 8200 ft. The main faults that were delineated on the seismic sections showed a clear NW–SE-trending fault (Red Sea System), which dips mainly to the SW, with some NE-dipping faults in the southern part forming horsts. The other major NE-SW and N-S fault patterns are thrown northwest ward. The isopach map showed that in the southeast and west sections the Matulla Formation, thickness increased and reached maximum thickness of 1100 ft, and decreased in the central and northeastern portions of the region platform reaching minimum thickness of less than 100 ft.
- Petrographic investigations of accessible core samples revealed that the Matulla sandstone reservoir samples were made up mostly of colorless-light gray sublithic arenite sandstone, which was medium- to fine-grained, sub-angular to sub-rounded, and moderately sorted. The Matulla sandstone is cemented by calcite, dolomite rhombs, argillaceous, and glauconitic minerals. The sandstone facies displayed good visual porosity, which reflects the Matulla sandstone's ability to store oil.
- The 3D facies model indicates that the Matulla Formation is made up mainly of 23% sandstone, 9.6% siltstone, 39.3% shale, 21.7% limestone, 2.6% dolomite and 3.8% calcareous shale.
- According to the petrophysical model, the Matulla Formation's upper and lower zones are good quality reservoir, while the middle zone is a poor quality reservoir. It was also deduced that lateral and vertical changes in petrophysical properties were linked to lateral and vertical changes in lithology across the complex Matulla reservoir.
- To better exploit the Matulla reservoir, the most favorable sectors in the Matulla reser-

voir for accumulation and production of hydrocarbons are likely at the central, southeast and southwest parts of the studied oilfield.

- We provided an overview of reservoir modeling issues, focusing on the complex geometry of the complex Matulla reservoir and the diverse reservoir parameters based on available data and the most likely extracted reservoir parameters.
- We combined multiple datasets and used the most likely parameters calibrated by core measurements to improve modeling of the complex Matulla reservoir and reduced the common uncertainties associated with the static modeling process.

ACKNOWLEDGMENTS

The authors would like to thank the Egyptian General Petroleum Corporation (EGPC) and Gulf of Suez Petroleum Company (GUPCO) for providing the dataset and permission to publish this work. Great thanks to the two anonymous reviewers and Prof. Dr. John Carranza, Editor-in-Chief of Natural Resources research for their comments and suggestions, which greatly benefited the manuscript. Many thanks to Prof. Karl Krainer from Innsbruck University and Prof. Cathy Hollis from Manchester University for revising the final version of this manuscript.

OPEN ACCESS

This article is licensed under a Creative Commons Attribution 4.0 International License, which permits use, sharing, adaptation, distribution and reproduction in any medium or format, as long as you give appropriate credit to the original author(s) and the source, provide a link to the Creative Commons licence, and indicate if changes were made. The images or other third party material in this article are included in the article's Creative Commons licence, unless indicated otherwise in a credit line to the material. If material is not included in the article's Creative Commons licence and your intended use is not permitted by statutory regulation or exceeds the permitted use, you will need to obtain

permission directly from the copyright holder. To view a copy of this licence, visit <http://creativecommons.org/licenses/by/4.0/>.

REFERENCES

- Abu Amarah, B. A., Nabawy, B. S., Shehata, A. M., Kassem, O. M., & Ghrefat, H. (2019). Integrated geological and petrophysical characterization of Oligocene deep marine nonconventional poor to tight sandstone gas reservoir. *Marine and Petroleum Geology*. <https://doi.org/10.1016/j.marpetgeo.2019.06.037>.
- Abd El-Gawad, E. A., Abdelwahhab, M. A., Bekiet, M. H., Noah, A. Z., ElSayed, N. A., & Fouda, A. E. E. (2019). Static reservoir modeling of El Wastani formation, for justifying development plans, using 2D seismic and well log data in Scarab field, offshore Nile Delta, Egypt. *Journal of African Earth Sciences*, 158, 103546.
- Abdel-Fattah, M., Dominik, W., Shendi, E., Gadallah, M., & Rashed, M. (2010). 3D integrated reservoir modeling for Upper Safa Gas Development in Obaiyed Field, Western Desert, Egypt. In *72nd EAGE conference and exhibition incorporating SPE EUROPEC*, Spain, June 2010. <https://doi.org/10.3997/2214-4609.201401358>.
- Abdel-Fattah, M. I., Metwalli, F. I., & Mesilhi, E. S. I. (2018). Static reservoir modeling of the Bahariya reservoirs for the oilfields development in South Umbarka area, Western Desert, Egypt. *Journal of African Earth Sciences*, 138, 1–13.
- Abdelghany, W. K., Radwan, A. E., Elkhawaga, M. A., Wood, D. A., Sen, S., & Kassem, A. A. (2021). Geomechanical modeling using the depth-of-damage approach to achieve successful underbalanced drilling in the Gulf of Suez Rift Basin. *Journal of Petroleum Science and Engineering*. <https://doi.org/10.1016/j.petrol.2020.108311>.
- Abdelmaksoud, A. (2017). *Integrated geological modeling of the upper Bahariya reservoir in Abu Gharadig oil and gas field, North Western Desert, Egypt*. M.Sc. Thesis, Faculty of Science, Assiut University, Egypt.
- Abdelmaksoud, A., Amin, A. T., El-Habaak, G. H., & Ewida, H. F. (2019a). Facies and petrophysical modeling of the Upper Bahariya Member in Abu Gharadig oil and gas field, north Western Desert, Egypt. *Journal of African Earth Sciences*, 149(C), 503–516.
- Abdelmaksoud, A., Ewida, H. F., El-Habaak, G. H., & Amin, A. T. (2019b). 3D structural modeling of the Upper Bahariya Member in Abu Gharadig oil and gas field, North Western Desert, Egypt. *Journal of African Earth Sciences*, 150(c), 685–700.
- Abudeif, A. M., Attia, M. M., Al-Khashab, H. M., & Radwan, A. E. (2018). Hydrocarbon type detection using the synthetic logs: A case study, Baba member, Gulf of Suez, Egypt. *Journal of African Earth Sciences*, 144, 176–182. <https://doi.org/10.1016/j.jafrearsci.2018.04.017>.
- Abudeif, A. M., Attia, M. M., & Radwan, A. E. (2016a). Petrophysical and petrographic evaluation of Sidri Member of Belayim Formation, Badri field, Gulf of Suez, Egypt. *Journal of African Earth Sciences*, 115, 108–120. <https://doi.org/10.1016/j.jafrearsci.2015.11.028>.
- Abudeif, A. M., Attia, M. M., & Radwan, A. E. (2016b). New simulation technique to estimate the hydrocarbon type for the two untested members of Belayim Formation in the absence of pressure data, Badri Field, Gulf of Suez, Egypt. *Arabian Journal of Geosciences*, 9(3), 1–21. <https://doi.org/10.1007/s12517-015-2082-2>.
- Agbasi, O. E., Igboekwe, M. U., Chukwu, G. U., & Sunday, E. E. (2018). Discrimination of pore fluid and lithology of a well in X Field, Niger Delta, Nigeria. *Arabian Journal of Geosciences*, 11(11), 1–7.
- Ali, M., Abdelhady, A., Abdelmaksoud, A., Darwish, M., & Essa, M. A. (2019a). 3D static modeling and petrographic aspects of the Albian/Cenomanian Reservoir, Komombo Basin, Upper Egypt. *Natural Resources Research*, 29, 1259–1281.
- Ali, M., Abdelmaksoud, A., Essa, M. A., Abdelhady, A., & Darwish, M. (2019b). 3D structural, facies and petrophysical modeling of C member of six hills formation, Komombo Basin, Upper Egypt. *Natural Resources Research*, 29, 2575–2597.
- Alsharhan, A. S. (2003). Petroleum geology and potential hydrocarbon play in the Gulf of Suez rift basin, Egypt. *AAPG Bulletin*, 87(1), 143–180.
- Alsharhan, A. S., & Salah, M. G. (1995). Geology and hydrocarbon habitat in rift setting: northern and central Gulf of Suez, Egypt. *Bulletin of Canadian Petroleum Geology*, 43(2), 156–176.
- Attia, M. M., Abudeif, A. M., & Radwan, A. E. (2015). Petrophysical analysis and hydrocarbon potentialities of the untested Middle Miocene Sidri and Baba sandstone of Belayim Formation, Badri field, Gulf of Suez, Egypt. *Journal of African Earth Sciences*, 109, 120–130. <https://doi.org/10.1016/j.jafrearsci.2015.05.020>.
- Avseth, P., Mukerji, T., & Mavko, G. (2005). *Quantitative seismic interpretation: Applying rock physics tools to reduce interpretation risk*. Cambridge University Press. <https://doi.org/10.1017/CBO9780511600074>.
- Baack, W., & Latif, M. (1995). Innovative use of horizontal wells in mature fields boosts production/reserves. *Proceedings SPE Middle East Oil Show, Bahrain*. <https://doi.org/10.2118/29882-MS>.
- Bilodeau, B., De, G., Wild, T., Zhou, Q., & Wu, H. (2002). Integrating formation evaluation into earth modeling and 3D petrophysics. In *SPWLA 43rd annual logging symposium*.
- Brown, R. N. (1980). History of exploration and discovery of El Morgan, Ramadan and July oilfields, Gulf of Suez, Egypt. *Memoir of the Canadian Society of Petroleum Geologists*, 6, 733–764.
- Bryant, I. D., & Flint, S. S. (1993). Quantitative clastic reservoir geological modeling: Problems and perspectives. In S. S. Flint & I. D. Bryant (Eds.), *The geological modeling of hydrocarbon reservoirs and outcrop analogues*. *International Association of Sedimentologists Special Publication* (Vol. 15, pp. 3–20). Wiley.
- Bryant, I. D., & Flint, S. S. (2009). *The geological modeling of hydrocarbon reservoirs and outcrop analogues (Special publication of the International Association of Sedimentologists)* (Vol. 37). Wiley.
- Cannon, S. (2018). *Reservoir modeling: A practical guide*. Wiley.
- Colletta, B., Le Quellec, P., Letouzey, J., & Moretti, I. (1988). Longitudinal evolution of the Suez Rift Structure (Egypt). *Tectonophysics*, 153, 221–233.
- Cosentino, L. (2005). Static reservoir study. In P. Barnaba (Ed.), *Encyclopaedia of hydrocarbons* (Vol. I, pp. 553–573). Marchesi Grafiche Editoriali S.p.a.
- Darwish, M., & El Araby, A. (1993). Petrography and diagenetic aspects of some siliclastic hydrocarbon reservoir in relation to the rifting of the Gulf of Suez, Egypt. *Geol. Soc. Egypt Spec. Publ*, 1, 155–187.
- Day, R. A., & Hoffman, K. S. (1997). GUPCO more efficiently taps Suez oil using 3-D modeling. *World Oil*, 218(9), 47–53.
- Dean, L. (2008). Volumetric estimation. In Mireault, R., & Dean, L. (Eds.), *Reservoir engineering for geologists*. Canadian Society of Petroleum Geologists Reservoir Magazine, 2011–2014. Accessed October 20, 2017.

- Deutsch, C. (2002). *Geostatistical reservoir modeling*. Oxford University Press: New York.
- Deutsch, C. V., & Journel, A. G. (1998). *Geostatistical software library and user's guide* (2nd ed., p. 369). Oxford University Press.
- Doyen, P. M. (2007). *Seismic reservoir characterization: An earth modeling perspective*. EAGE Publications.
- EGPC, Egyptian General Petroleum Corporation. (1996). Gulf of Suez oil fields (A comprehensive overview). Cairo, Egypt (pp. 484–495).
- El Khadragey, A. A., Eysa, E. A., Hashim, A., & Abd El Kader, A. (2017). Reservoir characteristics and 3D static modeling of the late Miocene Abu madi formation, onshore Nile delta, Egypt. *Journal of African Earth Sciences*, 132, 99–108.
- El Sharawy, M. S., & Nabawy, B. S. (2015). Geological and petrophysical characterization of the Coniacian–Santonian Matulla formation in Southern and Central Gulf of Suez, Egypt. *Arabian Journal for Science and Engineering*, 41, 281–300.
- El-Azabi, M. H., & El-Araby, A. (2007). Depositional framework and sequence stratigraphic aspects of the Coniacian–Santonian mixed siliciclastic/carbonate Matulla sediments in Nezzazat and Ekma blocks, Gulf of Suez, Egypt. *Journal of African Earth Sciences*, 47(4–5), 179–202.
- Elkhwaga, M. A., Elghaney, W., Naidu, R., Hussien, A., Rafaat, R., Baker, K., Radwan, A., & Julian, H. (2021). *Impact of high resolution 3D geomechanics on well optimization in the Southern Gulf of Suez, Egypt*. Paper presented at the SPE Annual Technical Conference and Exhibition, Dubai, UAE. <https://doi.org/10.2118/206271-MS>.
- El-Sabbagh, A., Tantawy, A. A., Keller, G., Khozyem, H., Spangenberg, J., Adatte, T., & Gertsch, B. (2011). Stratigraphy of the Cenomanian–Turonian oceanic anoxic event OAE2 in shallow shelf sequences of NE Egypt. *Cretaceous Research*, 32(6), 705–722.
- Fagin, S. W. (1991). *Seismic modeling of geologic structures: Applications to exploration problems*. *Geophysical Development Series* (Vol. 2, p. 269). Society of Exploration Geophysicists.
- Gaafar, G. R., Attia, G., Khaled, K. A., & Ibrahim, S. M. (2009). Petrophysical evaluation of Rudeis Reservoir in July Oil Field, Gulf of Suez, Egypt. In *Second international conference on the role of applied geology in environmental development* (pp. 1–21).
- Garfunkel, Z., & Bartov, Y. (1977). The tectonics of the Suez rift. *Geological Survey of Israel Bulletin*, 71, 44–71.
- Gartrell, A., Zhang, Y., Lisk, M., & Dewhurst, D. (2004). Fault intersections as critical hydrocarbon leakage zones: Integrated field study and numerical modeling of an example from the Timor Sea, Australia. *Journal of Marine and Petroleum Geology*, 21(9), 1165–1179.
- Godwill, P. A., & Waburoko, J. (2016). Application of 3D reservoir modeling on Zao 21 Oil Block of Zilaitun Oil Field. *Journal of Petroleum Environmental and Biotechnology*, 7, 262.
- Hasouba, M., Abd El Shafy, A., & Mohamed, A. (1992). Nezzazat Group—reservoir geometry and rock types in the October field area, Gulf of Suez. In *11th EGPC petroleum exploration and production conference 1* (pp. 293–317).
- Holden, L., Mostad, P., Nielsen, B. F., Gjerde, J., Townsend, C., & Ottesen, S. (2003). Stochastic structural modeling. *Journal of Mathematical Geology*, 35(8), 899–914.
- Hu, L. Y., & Ravalec-Dupin, M. L. (2005). On some controversial issues of geostatistical simulation. In O. Leuangthong & C. V. Deutsch (Eds.), *Geostatistics Banff 2004. Quantitative geology and geostatistics*. (Vol. 14). Dordrecht: Springer.
- Isaaks, E. H. (1991). *The application of Monte Carlo methods to the analysis of spatially correlated data*. Ph.D. Thesis, Stanford University.
- Islam, M. A., Yunsi, M., Qadri, S. T., Shalaby, M. R., & Haque, A. E. (2021). Three-dimensional structural and petrophysical modeling for reservoir characterization of the Mangahewa formation, Pohokura Gas-Condensate Field, Taranaki Basin, New Zealand. *Natural Resources Research*, 30(1), 371–394.
- Jika, H. T., Onuoha, M. K., Okeugo, C. G., & Eze, M. O. (2020). Application of sequential indicator simulation, sequential Gaussian simulation and flow zone indicator in reservoir-E modeling; Hatch Field Niger Delta Basin, Nigeria. *Arabian Journal of Geosciences*, 13, 410. <https://doi.org/10.1007/s12517-020-05332-8>.
- John, R. O., Adujo, A. A., & Taiwo, A. O. (2010). Applications of 3-D structural interpretation and seismic attribute analysis to hydrocarbon prospecting over X-field, Niger-Delta. *Int J Basic Appl Sci*, 10(4), 28–40.
- Journel, A. (1982). The indicator approach to estimation of spatial distributions. in *17th APCOM symposium proceedings. Society of mining engineers* (pp. 793–806).
- Kassem, A. A., Hussein, W. S., Radwan, A. E., Anani, N., Abioui, M., Jain, S., & Shehata, A. A. (2021a). Petrographic and diagenetic study of siliciclastic Jurassic sediments from the Northeastern Margin of Africa: Implication for reservoir quality. *Journal of Petroleum Science and Engineering*. <http://doi.org/10.1016/j.petrol.2020.108340>.
- Kassem, A. A., Sen, S., Radwan, A. E., Abdelghany, W. K., & Abioui, M. (2021b). Effect of depletion and fluid injection in the mesozoic and paleozoic sandstone reservoirs of the October Oil Field, Central Gulf of Suez Basin: Implications on drilling, production and reservoir stability. *Natural Resources Research*. <https://doi.org/10.1007/s11053-021-09830-8>.
- Kassem, A. A., Sharaf, L. M., Baghdady, A. R., & El-Naby, A. A. (2020). Cenomanian/Turonian oceanic anoxic event 2 in October oil field, central Gulf of Suez, Egypt. *Journal of African Earth Sciences*, 165, 103817.
- Marttila, R. K., & El Bahr, M. (1994). Evaluation of a lithology complex reservoir (Nezzazat Group) in the Gulf of Suez. In *12th EGPC exploration and production conference 2* (pp. 472–482).
- Mc Clay, K., Nichols, G., Khalil, S., Darwish, M., & Bosworth, W. (1998). Extensional tectonics and sedimentation, eastern Gulf of Suez, Egypt. In B. H. Purser & D. W. J. Bosence (Eds.), *Sedimentation and tectonics of rift basins, Red Sea-Gulf of Aden* (pp. 223–238). Chapman and Hall.
- Mutebi, S., Sen, S., Sserubiri, T., Rudra, A., Ganguli, S. S., & Radwan, A. E. (2021). Geological characterization of the Miocene–Pliocene succession in the Semliki Basin, Uganda: Implications for hydrocarbon exploration and drilling in the East African Rift System. *Natural Resources Research*. <http://doi.org/10.1007/s11053-021-09951-0>.
- Okoli, A. E., Agbasi, O. E., Lashin, A. A., & Sen, S. (2021). Static reservoir modeling of the Eocene Clastic Reservoirs in the Q-Field, Niger Delta, Nigeria. *Natural Resources Research*, 30, 1411–1425.
- Pettijohn, F. J., & Potter, P. E. (2012). *Atlas and glossary of primary sedimentary structures*. Springer.
- Poupon, A., & Leveaux, J. (1971). Evaluation of water saturation in shaly formations. In *Proceedings of the SPWLA 12th annual logging symposium*.
- Pyrzc, M. J., & Deutsch, C. V. (2014). *Geostatistical reservoir modeling* (2nd ed.). Oxford University Press.
- Qadri, S. T., Islam, M. A., & Shalaby, M. R. (2019). Three-dimensional petrophysical modeling and volumetric analysis to model the reservoir potential of the Kupe Field, Taranaki Basin, New Zealand. *Natural Resources Research*, 28(2), 369–392.
- Qadri, S. T., Islam, M. A., Shalaby, M. R., & Abd El-Aal, A. K. (2021). Reservoir quality evaluation of the Farewell sandstone by integrating sedimentological and well log analysis in

- the Kupe South Field, Taranaki Basin-New Zealand. *Journal of Petroleum Exploration and Production*, 11(1), 11–31.
- Qadri, S. T., Islam, M. A., Shalaby, M. R., & Ali, S. H. (2020). Integration of 1D and 3D modeling schemes to establish the Farewell Formation as a self-sourced reservoir in Kupe Field, Taranaki Basin, New Zealand. *Frontiers of Earth Science*. <https://doi.org/10.1007/s11707-020-0839-8>.
- Qadri, S. T., Islam, M. A., Shalaby, M. R., & Eahsanul- Haque, A. K. (2017). Seismic interpretation and structural modeling of Kupe field, Taranaki Basin, New Zealand. *Arabian Journal of Geosciences*, 10, 295. <https://doi.org/10.1007/s12517-017-3078-x>.
- Radwan, A. E. (2021a). Modeling the depositional environment of the sandstone reservoir in the Middle Miocene Sidri Member, Badri Field, Gulf of Suez Basin, Egypt: Integration of gamma-ray log patterns and petrographic characteristics of lithology. *Natural Resources Research*, 30, 431–449. <https://doi.org/10.1007/s11053-020-09757-6>.
- Radwan, A. E. (2021b). Modeling pore pressure and fracture pressure using integrated well logging, drilling based interpretations and reservoir data in the Giant El Morgan oil Field, Gulf of Suez, Egypt. *Journal of African Earth Sciences*. <https://doi.org/10.1016/j.jafrearsci.2021.104165>.
- Radwan, A. E. (2021). Integrated reservoir, geology, and production data for reservoir damage analysis: A case study of the Miocene sandstone reservoir, Gulf of Suez. *Egypt. Interpretation*, 9(4), 1–46. <https://doi.org/10.1190/int-2021-0039.1>.
- Radwan, A. E., Abudeif, A. M., Attia, M. M., & Mahmoud, M. A. (2019c). Development of formation damage diagnosis workflow, application on Hammam Faraun reservoir: A case study, Gulf of Suez, Egypt. In *Offshore Mediterranean conference*. ISBN 9788894043679-2019.
- Radwan, A. E., & Sen, S. (2021d). *Stress path analysis of the depleted middle miocene clastic reservoirs in the Badri Field, Gulf of Suez Rift Basin, Egypt*. Paper presented at the SPE annual technical conference and exhibition, Dubai, UAE. <https://doi.org/10.2118/205900-MS>.
- Radwan, A. E., & Sen, S. (2021c). *Stress path analysis of the depleted miocene clastic reservoirs in the El Morgan Oil Field, Offshore Egypt*. Paper presented at the 55th U.S. Rock mechanics/geomechanics symposium.
- Radwan, A. E. (2022). Chapter 2 Three-dimensional gas property geological modeling and simulation. In A. D. Wood & J. Cai (Eds.) *Sustainable geoscience for natural gas sub-surface systems*, Elsevier. pp. 29-45. <https://doi.org/10.1016/B978-0-323-85465-8.00011-X>.
- Radwan, A. E., Abdelghany, W. K., & Elkhawaga, M. A. (2021d). Present-day in-situ stresses in Southern Gulf of Suez, Egypt: Insights for stress rotation in an extensional rift basin. *Journal of Structural Geology*, 147, 104334. <https://doi.org/10.1016/j.jsg.2021.104334>.
- Radwan, A. E., Abudeif, A. M., & Attia, M. M. (2020c). Investigative petrophysical fingerprint technique using conventional and synthetic logs in siliciclastic reservoirs: A case study, Gulf of Suez basin, Egypt. *Journal of African Earth Sciences*, 167, 103868. <https://doi.org/10.1016/j.jafrearsci.2020.103868>.
- Radwan, A. E., Abudeif, A. M., Attia, M. M., Elkhawaga, M. A., Abdelghany, W. K., & Kasem, A. A. (2020a). Geopressure evaluation using integrated basin modeling, well-logging and reservoir data analysis in the northern part of the Badri oil field, Gulf of Suez, Egypt. *Journal of African Earth Sciences*, 162, 103743. <https://doi.org/10.1016/j.jafrearsci.2019.103743>.
- Radwan, A. E., Abudeif, A. M., Attia, M. M., & Mahmoud, M. A. (2019a). Development of formation damage diagnosis workflow, application on Hammam Faraun reservoir: A case study, Gulf of Suez, Egypt. *Journal of African Earth Sciences*, 153, 42–53. <https://doi.org/10.1016/j.jafrearsci.2019.02.012>.
- Radwan, A. E., Abudeif, A. M., Attia, M. M., & Mohammed, M. A. (2019b). Pore and fracture pressure modeling using direct and indirect methods in Badri Field, Gulf of Suez, Egypt. *Journal of African Earth Sciences*, 156, 133–143. <https://doi.org/10.1016/j.jafrearsci.2019.04.015>.
- Radwan, A. E., Kassem, A. A., & Kassem, A. (2020b). Radwany Formation: A new formation name for the Early-Middle Eocene carbonate sediments of the offshore October oil field, Gulf of Suez: Contribution to the Eocene sediments in Egypt. *Marine and Petroleum Geology*, 116, 104304. <https://doi.org/10.1016/j.marpetgeo.2020.104304>.
- Radwan, A. E., Nabawy, B. S., Kassem, A. A., & Hussein, W. S. (2021b). Implementation of rock typing on waterflooding process during secondary recovery in oil reservoirs: A case study, El Morgan Oil Field, Gulf of Suez, Egypt. *Natural Resources Research*. <https://doi.org/10.1007/s11053-020-09806-0>.
- Radwan, A. E., Rohais, S., & Chiarella, D. (2021c). Combined stratigraphic-structural play characterization in hydrocarbon exploration: A case study of Middle Miocene sandstones, Gulf of Suez basin, Egypt. *Journal of Asian Earth Sciences*, 218, 104686. <https://doi.org/10.1016/j.jseaes.2021.104686>.
- Radwan, A., & Sen, S. (2021a). Stress path analysis for characterization of in situ stress state and effect of reservoir depletion on present-day stress magnitudes: Reservoir geomechanical modeling in the Gulf of Suez Rift Basin, Egypt. *Natural Resources Research*, 30, 463–478. <https://doi.org/10.1007/s11053-020-09731-2>.
- Radwan, A. E., & Sen, S. (2021b). Characterization of in-situ stresses and its implications for production and reservoir stability in the depleted El Morgan hydrocarbon field, Gulf of Suez Rift Basin, Egypt. *Journal of Structural Geology*, 148, 104355. <https://doi.org/10.1016/j.jsg.2021.104355>.
- Radwan, A. E., Trippetta, F., Kassem, A. A., & Kania, M. (2021a). Multi-scale characterization of unconventional tight carbonate reservoir: Insights from October oil field, Gulf of Suez rift basin, Egypt. *Journal of Petroleum Science and Engineering*, 197, 107968. <https://doi.org/10.1016/j.petrol.2020.107968>.
- Radwan, A. E., Wood, D. A., Abudeif, A. M., Attia, M. M., Mahmoud, M., Kassem, A. A., & Kania, M. (2021e). Reservoir formation damage; reasons and mitigation: A case study of the Cambrian-Ordovician Nubian 'C' sandstone oil and gas reservoir from the Gulf of Suez Rift Basin. *Arabian Journal for Science and Engineering*. <https://doi.org/10.1007/s13369-021-06005-8>.
- Radwan, A. E., Wood, D. A., Mahmoud, M., & Tariq, Z. (2022). Gas adsorption and reserve estimation for conventional and unconventional gas resources. In D. A. Wood & J. Cai (Eds.), *Sustainable geoscience for natural gas sub-surface systems* (pp. 345–382). Elsevier. <https://doi.org/10.1016/B978-0-323-85465-8.00004-2>.
- Remy, N., Boucher, A., & Wu, J. B. (2009). *Applied geostatistics with SGeMS* (p. 264). Cambridge University Press.
- Said, R. (1990). *Geology of Egypt* (p. 743). A. A. Balkema. <https://doi.org/10.1017/S0016756800019828>.
- Seifert, D., & Jensen, J. L. (1999). Using sequential indicator simulation as a tool in reservoir description: Issues and uncertainties. *Mathematical Geology*, 31, 527–550.
- Shehata, A. A., Kassem, A. A., Brooks, H. L., Zuchuat, V., & Radwan, A. E. (2021). Facies analysis and sequence-stratigraphic control on reservoir architecture: Example from mixed carbonate/siliciclastic sediments of Raha Formation, Gulf of Suez, Egypt. *Marine and Petroleum Geology*, 131, 105160. <https://doi.org/10.1016/j.marpetgeo.2021.105160>.
- Singh, V., Hegazy, M., & Fontanelli, L. (2009). Assessment of reservoir uncertainties for development evaluation and risk analysis. *The Leading Edge*, 28(3), 260–268.

Tyson, S. (2007). *An introduction to reservoir modeling*. Pipers' Ash, Limited.

Wu, Q., & Xu, H. (2004). On three-dimensional geological modeling and visualization, Science in China. *Series D Earth Sciences*, 47(8), 739–748.

Wu, L., Wang, Y., Chi, D., Xu, L., Chen, X., Jiang, Y., & Shi, W. (2005). An object-oriented 3D integral data model for digital

city and digital mine. Conference: MIPPR 2005 Geospatial Information, Data Mining, and Applications.

Yan-lin, S., Ai-ling, Z., You-bin, H., & Ke-yan, X. (2011). 3D geological modeling and its application under complex geological conditions. *Procedia Engineering*, 12, 41–46.